Draft of Technical Manual for Strata

Albert R. Kottke and Ellen M. Rathje

November 23, 2011

Contents

Contents i

List of Figures iii

List of Tables v

1 Introduction 1

2 Site Response Analysis 2
- 2.1 Equivalent Linear Site Response Analysis . . . 2
  - 2.1.1 Linear Elastic Wave Propagation . . . 2
  - 2.1.2 Equivalent-Linear Analysis . . . 8
  - 2.1.3 Dynamic Soil Properties . . . 10
- 2.2 Site Response Methods . . . 15
  - 2.2.1 Time Series Method . . . 15
  - 2.2.2 Random Vibration Theory Method . . . 16

3 Variation of Site Properties 28
- 3.1 Introduction . . . 28
- 3.2 Random Variables . . . 29
- 3.3 Statistical Models for Soil Properties . . . 32
  - 3.3.1 Layering and Velocity Model . . . 32
  - 3.3.2 Depth to Bedrock Model . . . 43
  - 3.3.3 Non-Linear Soil Properties Model . . . 43

4 Using Strata 45
- 4.1 Strata Particulars . . . 45
  - 4.1.1 Auto-Discretization of Layers . . . 45
  - 4.1.2 Interaction with Tables . . . 46
  - 4.1.3 Non-Linear Curves . . . 47

4.1.4 Recorded Motion Dialog 49
4.1.5 Output Widget 54
4.2 Examples 54
4.2.1 Example 1: Basic time domain 56
4.2.2 Example 2: RVT and Site Variation 59

Bibliography **62**

Index **65**

List of Figures

2.1 The notation used in the wave equation 3
2.2 Nomenclature for the theoretical wave propagation. 4
2.3 The input to surface transfer functions site in Table 2.1 considering different types of input. 6
2.4 *Outcrop* describes upward and downward waves being equal, *within* is used when the upward and downward waves are not equal. 7
2.5 An example of the strain-time history and effective strain (γ_{eff}). 9
2.6 An example shear-wave velocity profile 11
2.7 Examples of shear modulus reduction and material damping curves for soil. 12
2.8 The nonlinear soil properties predicted by the Darendeli (2001) model. 13
2.9 The mean and mean $\pm\sigma$ nonlinear soil properties predicted by Darendeli (2001). 14
2.10 Time domain method sequence 17
2.11 The comparison between the target response spectrum and the response spectrum computed with RVT. 23
2.12 The FAS computing through the inversion process. 23
2.13 The relative error between the computed response spectra and the target response spectrum. 24
2.14 RVT method sequence 26

3.1 Using a random variable from a uniform distribution between 0 and 1 to generate a variable from a distribution with a zero mean and unit standard deviation. 30
3.2 Two variables with a correlation coefficient of: (a) 0.0, (b), 0.99, and (c) -0.7. 31

3.3 A layering profile consisting of 8 layers modeled by a homogeneous Poisson process with a rate of 1. 34
3.4 Toro (1995) layering model. (a) The occurrence rate (λ) as a function of depth (d), and (b) the expected layer thickness (h) as a function of depth. 35
3.5 Transformation between a homogeneous Poisson process with rate 1 to the Toro (1995) non-homogeneous Poisson process. 36
3.6 A layering simulated with the non-homogeneous Poisson process defined by Toro (1995). 36
3.7 Ten generated shear-wave velocity (v_s) profiles for a USGS C site class. (a) Using generic layering and median v_s, (b) using user defined layering and median v_s. 42
3.8 Generated nonlinear properties assuming perfect negative correlation. 44

4.1 Strata location selection 46
4.2 By clicking on the button circled in red all rows in the table are selected. 48
4.3 The nonlinear curve manager. 50
4.4 The initial view of the `Recorded Motion Dialog`. 52
4.5 An example a completed `Recorded Motion Dialog`. 53
4.6 Using the Output view to examine the results of a calculation. 55
4.7 The shear-wave velocity profile of the Sylmar County Hospital Parking Lot site (Chang, 1996). 56
4.8 Settings to enable RVT site response and variation of the shear-wave velocity. 60

List of Tables

2.1 The site properties of an example site. 5
2.2 The values of the RVT calculation for the input motion. . . . 25
2.3 The values of the RVT calculation for the input and surface motions. 27

3.1 The categories of the geotechnical subsurface conditions (third letter) in the Geomatrix site classification (Toro, 1995). 39
3.2 The USGS site categories, where $\overline{v}_{s,30}$ is the time weighted average shear-velocity of the top 30 m (Toro, 1995). 39
3.3 Coefficients for the Toro (1995) model, calculated by maximum likelihood. 40
3.4 Median shear-wave velocity (m/s) based on the generic site classification. 41

4.1 Soil profile at the Sylmar County Hospital Parking Lot site (Chang, 1996). The mean effective stress (σ'_m) is computed assuming a k_0 of 1/2 and a water table depth of 46 meters. 57

Chapter 1

Introduction

The computer program Strata performs equivalent linear site response analysis in the frequency domain using time domain input motions or random vibration theory (RVT) methods, and allows for randomization of the site properties. The following document explains the technical details of the program, as well as provides a user's guide to the program.

Strata is distributed under the GNU General Public License which can be found here:`http://www.gnu.org/licenses/`. Financial support was provided by the Pacific Earthquake Engineering Research Center under ???.

Chapter 2

Site Response Analysis

Strata computes the dynamic site response of a one-dimensional soil column using linear wave propagation with strain dependent dynamic soil properties. This is commonly referred as equivalent linear analysis method, which was first used in the computer program `SHAKE` (Idriss and Sun, 1992; Schnabel et al., 1972). Similar to `SHAKE`, Strata only computes the response for vertically propagating, horizontally polarized shear waves propagated through a site with horizontal layers.

The following chapter introduces strain dependent soil properties, linear-elastic wave propagation through a layered medium, and the equivalent linear approach to site response analysis.

2.1 Equivalent Linear Site Response Analysis

2.1.1 Linear Elastic Wave Propagation

For linear elastic, one-dimensional wave propagation, the soil is assumed to behave as a Kelvin-Voigt solid, in which the dynamic response is described using a purely elastic spring and a purely viscous dashpot (Kramer, 1996). The solution to the one-dimensional wave equation for a single wave frequency (ω) provides displacement (u) as a function of depth (z) and time (t) (**?**):

$$u(z,t) = A \exp\left[i\left(\omega t + k^* z\right)\right] + B \exp\left[i\left(\omega t - k^* z\right)\right] \tag{2.1}$$

In equation (2.1), A and B represent the respective amplitudes of the upward ($-z$) and downward ($+z$) waves, respectively (Figure 2.1). The complex wave number (k^*) in equation (2.2) is related to the shear modulus (G),

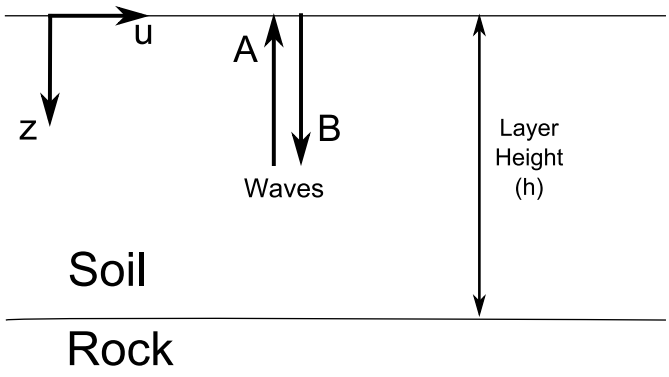

Figure 2.1: The notation used in the wave equation

damping ratio (D), and mass density (ρ) of the soil using:

$$k^* = \frac{\omega}{v_s^*} \tag{2.2}$$

$$v_s^* = \sqrt{\frac{G^*}{\rho}} \tag{2.3}$$

$$G^* = G\left(1 - 2D^2 + \imath 2D\sqrt{1 - D^2}\right) \simeq G(1 + \imath 2D) \tag{2.4}$$

G^* and v_s^* are called the complex shear modulus and complex shear-wave velocity, respectively. If the damping ratio (D) is small ($< 10 - 20\%$), then the approximation of the complex shear modulus in equation (2.4) is appropriate. Strata uses the complete definition of the complex shear-modulus, not the approximation, in the calculations.

Equation 2.1 applies only to a single layer with uniform soil properties and the wave amplitudes (A and B) can be computed from the layer boundary conditions. For a layered system, shown in Figure 2.2, the wave amplitudes are calculated using recursive formulas developed by maintaining compatibility of displacement and shear stress at the layer boundaries. Using these assumptions, the following recursive formulas are developed (Kramer, 1996):

$$\begin{aligned} A_{m+1} &= \tfrac{1}{2}A_m\left(1 + \alpha_m^*\right)\exp\left(\imath k_m^* h_m\right) + \tfrac{1}{2}B_m\left(1 - \alpha_m^*\right)\exp\left(-\imath k_m^* h_m\right) \\ B_{m+1} &= \tfrac{1}{2}A_m\left(1 - \alpha_m^*\right)\exp\left(\imath k_m^* h_m\right) + \tfrac{1}{2}B_m\left(1 + \alpha_m^*\right)\exp\left(-\imath k_m^* h_m\right) \end{aligned} \tag{2.5}$$

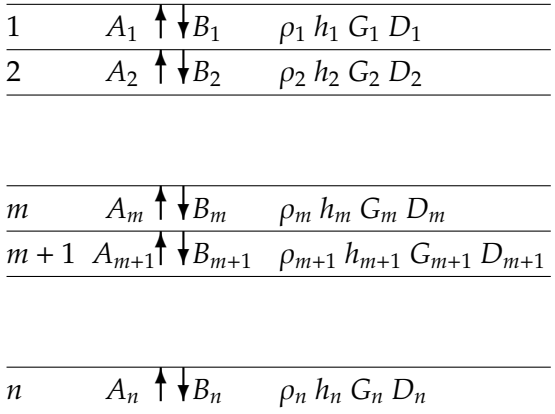

Figure 2.2: Nomenclature for the theoretical wave propagation.

where m is the layer number, h_m is the layer height and α_m^* is the complex impedance ratio. The complex impedance ratio is defined as:

$$\alpha_m^* = \frac{k_m^* G_m^*}{k_{m+1}^* G_{m+1}^*} = \frac{\rho_m v_{s,m}^*}{\rho_{m+1} v_{s,m+1}^*} \tag{2.6}$$

and quantifies the relative amplitudes of the upward and downward waves. At the surface of the soil column ($m = 1$), the shear stress must equal zero, therefore the amplitudes of the upward and downward waves must be equal ($A_1 = B_1$).

The wave amplitudes (A and B) within the soil profile are calculated at each frequency (assuming known stiffness and damping within each layer) and used to computed the response at the surface of a site. This calculation is performed by setting $A_1 = B_1 = 1.0$ at the surface and recursively calculating the wave amplitudes (A_{m+1},B_{m+1}) in successive layers until the input (base) layer is reached. The transfer function between the motion in the layer of interest (m) and in the rock layer (n) at the base of the deposit is defined as:

$$TF_{m,n}(\omega) = \frac{u_m(\omega)}{u_n(\omega)} = \frac{A_m + B_m}{A_n + B_n} \tag{2.7}$$

where ω is the frequency of the harmonic wave. The transfer function is the ratio of the amplitude of motion–either displacement, velocity, or acceleration–between two layers of interest and varies with frequency. The transfer function for the site with the properties presented in Table 2.1 is

Property	**Rock**	**Soil**
Mass Density (ρ)	2.24 g/cm^3	1.93 g/cm^3
Height (h)	inf	50 m
Shear-wave Velocity (v_s)	1500 m/s	350 m/s
Damping ratio (D)	1%	7%

Table 2.1: The site properties of an example site.

shown in Figure 2.3. The locations of the peaks in the transfer function are controlled by the modes of vibration of the soil deposit. The peak at the lowest frequency represents the fundamental (i.e. first) mode of vibration and results in the largest amplification. The peaks at higher frequencies are the higher vibrational modes of the site. The first natural frequency of a site is inversely related to the site period, where the site period is defined as (Kramer, 1996):

$$T_s = \frac{4 \cdot h_{soil}}{\overline{v}_s} \tag{2.8}$$

In equation (2.8), h_{soil} is the total height of the soil and $\overline{v}_s$ average velocity of the site.

$$2 + 2 = 4 \tag{2.9}$$

For the example site (Table 2.1), the site period is calculated to be 0.57 s which corresponds to a natural frequency of 1.75 Hz. In the transfer function (Figure 2.3), the peak with the highest amplification occurs at this frequency. The amplitudes of the peaks are controlled by the damping ratio of the soil. As the damping of the system increases, the amplitudes of the peaks decrease, which results in less amplification at the surface.

The response at the layer of interested is computed by multiplying the Fourier amplitude spectrum of the input rock motion by the transfer function:

$$Y_m(\omega) = TF_{m,n}(\omega) \cdot Y_n(\omega) \tag{2.10}$$

where Y_n is the input Fourier amplitude spectrum at layer n and Y_m is the Fourier amplitude spectrum at the top of the layer of interest. The Fourier amplitude spectrum of the input motion can be defined using a variety of methods and is discussed further in Sections 2.2.1 and 2.2.2.

One issue that must be considered is that the input Fourier spectrum typically represents a motion at the ground surface, where the upgoing and downgoing wave amplitudes are equal ($A_1 = B_1$), not at the base of a soil

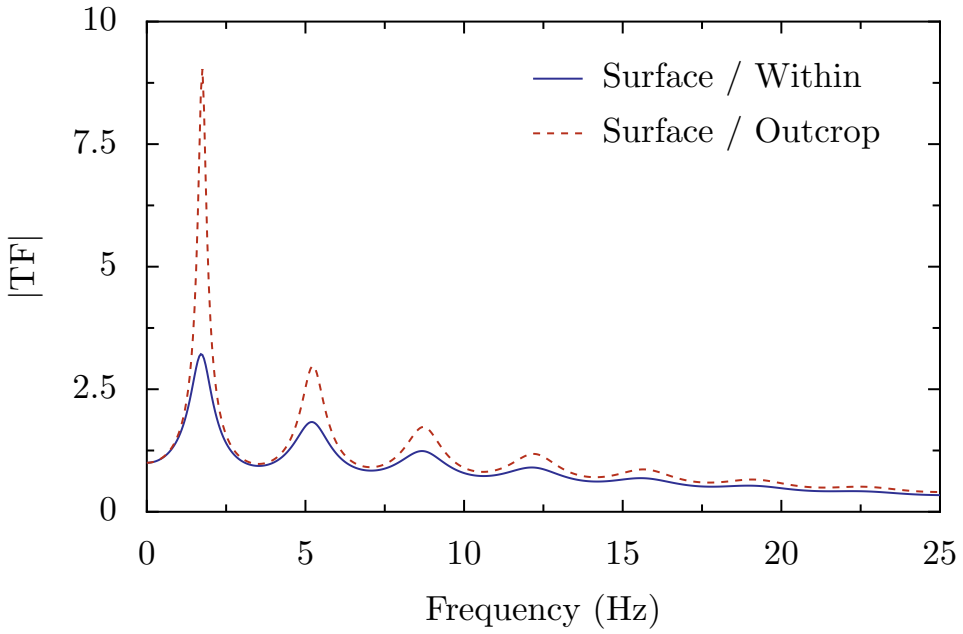

Figure 2.3: The input to surface transfer functions site in Table 2.1 considering different types of input.

deposit, where the wave amplitudes are not equal (Figure 2.4). The change in boundary conditions ($A_n = B_n$ for the surface, $A_n \neq B_n$ at the base of a soil deposit) must be taken into account. The motions at any free surface are referred to as *outcrop* motions and their amplitudes are described by twice the amplitude of the upward wave ($2A$). Equation (2.7) can be modified to transfer an outcrop motion to a surface motion. This result is obtained by multiplying equation (2.7) by a transfer function that takes the outcrop motions and makes it a within motion at the base of the soil column.

to an *outcrop* motion a second transfer function is required to translate from an *outcrop* motion to a *within* motion. The combined transfer function is defined as:

$$TF_{m,n}(\omega) = \underbrace{\frac{A_n + B_n}{2 \cdot A_n}}_{outcrop \rightarrow within} \cdot \underbrace{\frac{A_m + B_m}{A_n + B_n}}_{within \rightarrow layer_n} = \underbrace{\frac{A_m + B_m}{2 \cdot A_n}}_{outcrop \rightarrow layer_n} \tag{2.11}$$

Motions recorded at depth (e.g. recorded in a borehole) are referred to as *within* motions and for these motions the transfer function given in

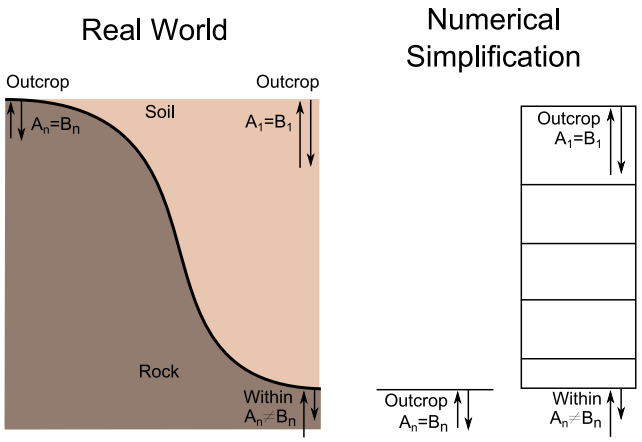

Figure 2.4: *Outcrop* describes upward and downward waves being equal, *within* is used when the upward and downward waves are not equal.

equation (2.7) can be used.

Figure 2.3 shows the transfer function for the site profile presented in Table 2.1 using equation (2.11 where the input motion is specified as *outcrop*. In comparison with the *within*-to-*outcrop* transfer function, the *outcrop*-to-*outcrop* transfer function displays less amplification for all modes.

2.1.2 Equivalent-Linear Analysis

The previous section assumed that the soil was linear-elastic. However, soil is nonlinear, such that the dynamic properties of soil (shear modulus, G, and damping ratio, D) vary with shear strain, and thus the intensity of shaking. In equivalent-linear site response analysis, the nonlinear response of the soil is approximated by modifying the linear elastic properties of the soil based on the induced strain level. Because the induced strains depend on the soil properties, the strain compatible shear modulus and damping ratio values are iteratively calculated based on the computed strain.

A transfer function is used to compute the shear strain in the layer based on the outcropping input motion. In the calculation of the strain transfer function, the shear strain is computed at the middle of the layer ($z = h_m/2$) and used to select the strain compatible soil properties. Unlike the previous transfer functions that merely amplified the Fourier amplitude spectrum, the strain transfer function amplifies the motion and converts acceleration into strain. The strain transfer function based on an outcropping input motion is defined by:

$$TF^{strain}_{mn}(\omega) = \frac{\gamma(\omega, z = h_m/2)}{\ddot{u}_{n,outcrop}(\omega)} = \frac{\imath k_m \left[A_m \exp\left(\imath k^*_m h_m/2\right) - B_m \exp\left(-\imath k^*_m h_m/2\right)\right]}{-\omega^2 \left(2 \cdot A_n\right)} \tag{2.12}$$

The strain Fourier amplitude spectrum within a layer is calculated by applying the strain transfer function to the Fourier amplitude spectrum of the input motion. The maximum strain within the layer is derived from this Fourier amplitude spectrum – either through conversion to the time domain or through RVT methods, further discussed in Section 2.2). However, it is not appropriate to use the maximum strain within the layer to compute the strain-compatible soil properties, because the maximum strain only occurs for an instant in time. Instead, an effective strain (γ_{eff}) is calculated from the maximum strain. Typically, the effective strain is 65% of the maximum strain. An example of a strain time-series and the effective strain is shown in Figure 2.5.

Equivalent-linear site response analysis requires that the strain dependent nonlinear properties (i.e. G and D) be defined. The initial (small strain) shear modulus (G_{max}) is calculated by:

$$G_{max} = \rho v_s^2 \tag{2.13}$$

where ρ is the mass density of the site, and v_s is the measured shear-wave velocity. Characterizing the nonlinear behavior of G and D is achieved

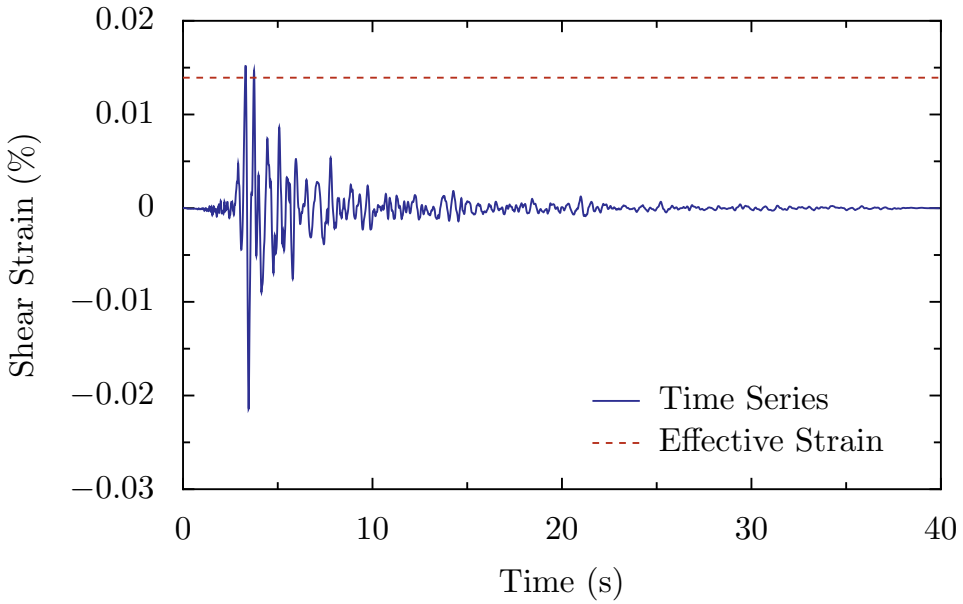

Figure 2.5: An example of the strain-time history and effective strain (γ_{eff}).

through modulus reduction and damping curves that describe the variation of G/G_{max} and D with shear strain (discussed in the next section). Using the initial dynamic properties of the soil, equivalent-linear site response analysis involves the following steps:

1. The wave amplitudes (A and B) are computed for each of the layers
2. The strain transfer function is calculated for each of the layers.
3. The maximum strain within each layer is computed by applying the strain transfer function to the input Fourier amplitude spectrum and finding the maximum response (see Section 2.2).
4. The effective strain (γ_{eff}) is calculated from the maximum strain within each layer.
5. The strain compatible shear modulus and damping ratio are recalculated based on the new estimate of the effective strain within each layer.

6. The new nonlinear properties (G and D) are compared to the previous iteration and an error is calculated. If the error for all layers is below a defined threshold the calculation stops.

After the iterative portion of the program finishes, the dynamic response of the soil deposit is computed.

2.1.3 Dynamic Soil Properties

In a dynamic system, the properties that govern the response are the mass, stiffness, and damping. In soil under seismic shear loading, the mass of the system is characterized by the mass density (ρ) and the layer height (h), the stiffness is characterized by the shear modulus (G), and the damping is characterized by the viscous damping ratio (D). The dynamic behavior of soil is challenging to model because it is nonlinear, such that, both the stiffness and damping of the system change with shear strain. Section 2.1.2 introduced equivalent-linear site response analysis in which the nonlinear response of the soil was simplified into a linear system that used strain-compatible dynamic properties (G and D). The analysis requires that the strain dependence of the nonlinear properties within a layer be fully characterized.

Defining the mass density of the system is a straight forward process because the density of soil falls within a limited range for soil and a good estimate of the mass density can be made based on soil type alone. Characterization of the stiffness and damping properties of soil is more complicated, the most rigorous approach requiring testing in both the field and laboratory.

The shear modulus and material damping of the soil are characterized using the small strain shear modulus (G_{max}), modulus reduction curves that relate G/G_{max} to shear strain, and damping ratio curves that relate D to shear strain. The small strain shear modulus is best characterized by in situ measurement of the shear-wave velocity as a function of depth. An example shear-wave velocity profile is shown in Figure 2.6. The profile tends to be separated into discrete layers with a generally increasing shear-wave velocity with increasing depth. Examples of modulus reduction and damping curves for soil are shown in Figure 2.7. These curves show a decrease in the soil stiffness and an increase in the damping ratio with an increase in shear strain.

The modulus reduction and damping curves may be obtained from laboratory measurements on soil samples or derived from empirical models

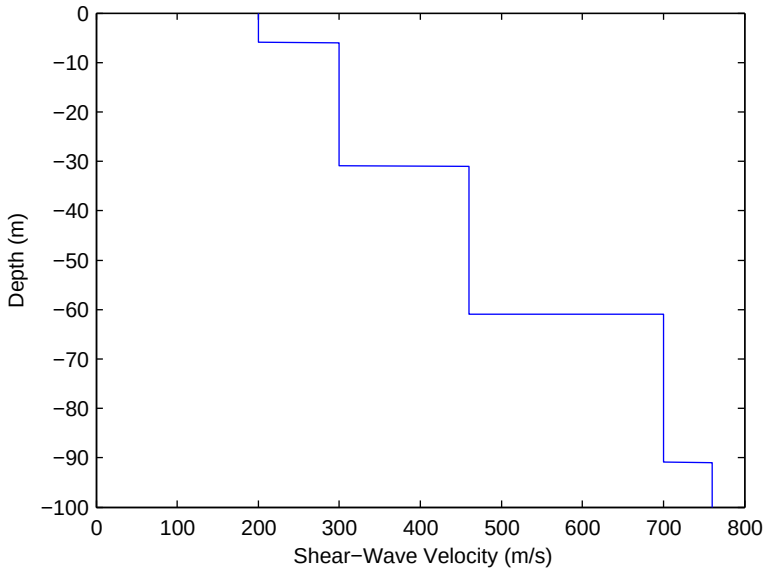

Figure 2.6: An example shear-wave velocity profile

based on soil type and other variables. One of the most comprehensive empirical models was developed by Darendeli (2001) and is included with Strata. The model expands on the hyperbolic model presented by Hardin and Drnevich (1972) and accounts for the effects of confining pressure (σ'_0), plasticity index (PI), over-consolidation ratio (OCR), frequency (f), and number of cycles of loading (N) on the modulus reduction and damping curves.

In the Darendeli (2001) model, the shear modulus reduction curve is a hyperbola defined by:

$$\frac{G}{G_{max}} = \frac{1}{1 + \left(\frac{\gamma}{\gamma_r}\right)^a} \tag{2.14}$$

where a is 0.9190, γ is the shear strain and γ_r is the reference shear strain. The reference shear strain (not in percent) is computed from:

$$\gamma_r = \left(\frac{\sigma'_0}{p_a}\right)^{0.3483} \left(0.0352 + 0.0010 \cdot PI \cdot OCR^{0.3246}\right) \tag{2.15}$$

where σ'_0 is the mean effective stress and p_a is the atmospheric pressure in atm. In the model, the damping ratio is calculated from the minimum

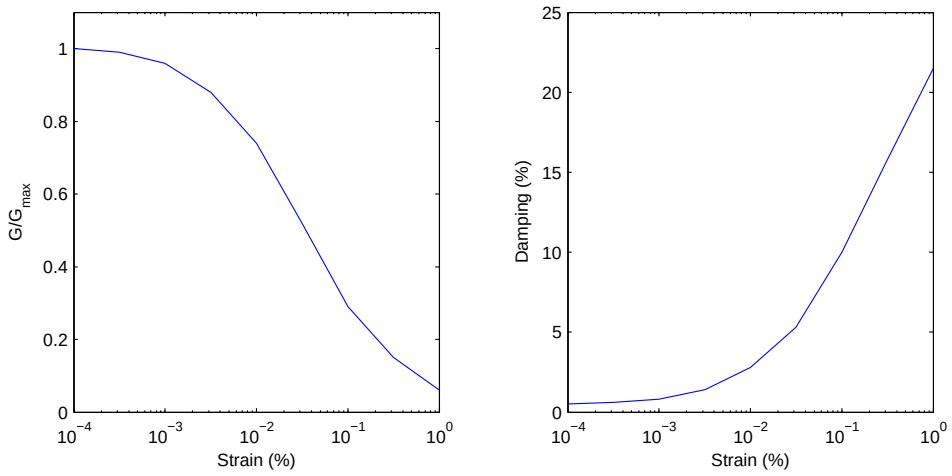

Figure 2.7: Examples of shear modulus reduction and material damping curves for soil.

damping ratio at small strains (D_{min}) and from the damping ratio associated with hysteretic Masing behavior (D_{Masing}). The minimum damping is calculated from:

$$D_{min}(\%) = (\sigma_0')^{-0.2889}\left(0.8005 + 0.0129 \cdot PI \cdot OCR^{-0.1069}\right)\left[1 + 0.2919 \ln(f)\right] \tag{2.16}$$

where f is the excitation frequency (Hz). The computation of the Masing damping requires the calculation of the area within the stress-strain curve predicted by the shear modulus reduction curve. The integration can be approximated by:

$$D_{\text{Masing}}(\%) = c_1 D_{\text{Masing},a=1} + c_2 D^2_{\text{Masing},a=1} + c_3 D^2_{\text{Masing},a=1} \tag{2.17}$$

where:

$$D_{masing,a=1}(\%) = \frac{100}{\pi}\left\{4\left[\frac{\gamma - \gamma_r \ln\left(\frac{\gamma+\gamma_r}{\gamma_r}\right)}{\frac{\gamma^2}{\gamma+\gamma_r}}\right] - 2\right\} \tag{2.18}$$

$$\begin{aligned} c_1 &= -1.1143a^2 + 1.8618a + 0.2533 \\ c_2 &= 0.0805a^2 - 0.0710a - 0.0095 \\ c_3 &= -0.0005a^2 + 0.0002a + 0.0003 \end{aligned} \tag{2.19}$$

The minimum damping ratio in equation (2.16) and the Masing damping in

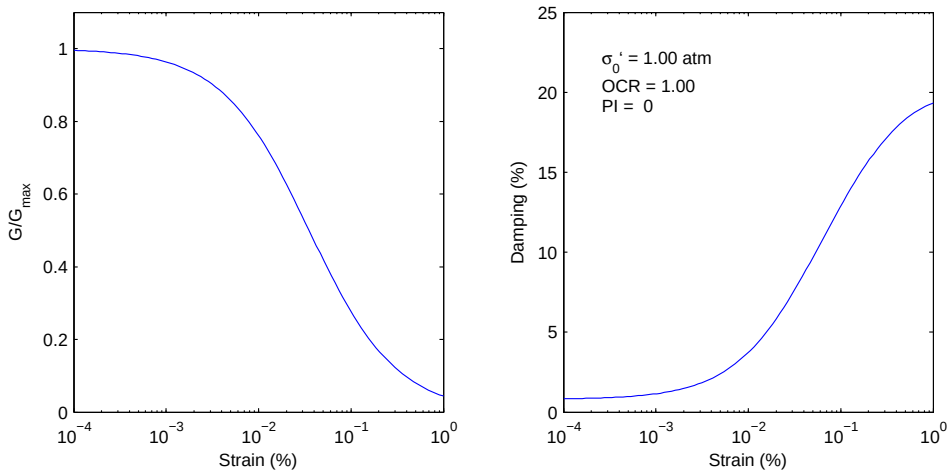

Figure 2.8: The nonlinear soil properties predicted by the Darendeli (2001) model.

equation (2.17) are combined to compute the total damping ratio (D) using:

$$D = b\left(\frac{G}{G_{max}}\right)^{0.1} \cdot D_{Masing} + D_{min} \tag{2.20}$$

where b is defined as:

$$b = 0.6329 - 0.0057 \ln(N) \tag{2.21}$$

where N is the number of cycles of loading. In most site response applications, the number of cycles (N) and the excitation frequency (f) in the model are defined as 10 and 1, respectively. Figure 2.8 shows the predicted nonlinear curves for a sand ($PI = 0, OCR = 1$) at an effective confining pressure of 1 atm.

A Bayesian approach was used in the Darendeli (2001) model to calculate the model coefficients. One of the unique aspects of this model is that the scatter of the data about the mean estimate is quantified. In the Darendeli (2001) model, the variability about the mean value is assumed to be normally distributed. The normal distribution is described using a mean and standard deviation. The mean values are calculated from equations (2.14) and (2.20). The standard deviation is a function of the amplitude of the nonlinear property (i.e. G/G_{max} and D). The standard deviation of the

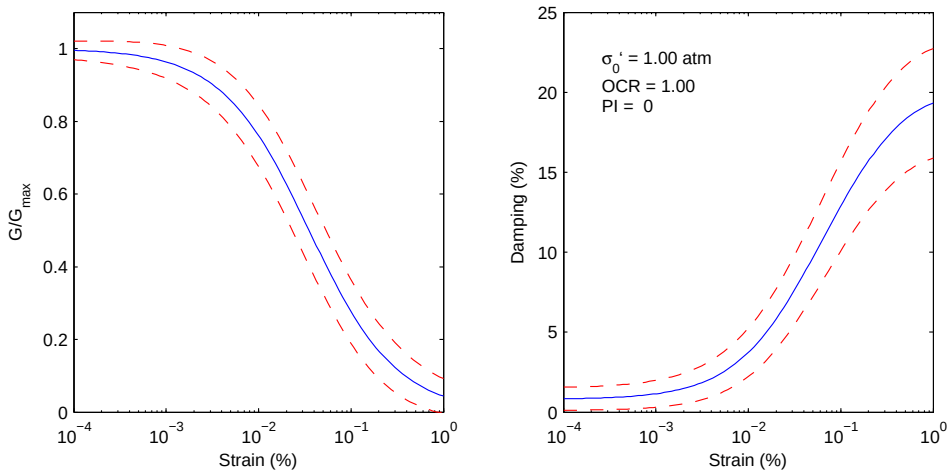

Figure 2.9: The mean and mean $\pm\sigma$ nonlinear soil properties predicted by Darendeli (2001).

normalized shear modulus (σ_{NG}) is computed by:

$$\sigma_{NG} = \exp(-4.23) + \sqrt{\frac{0.25}{\exp(3.62)} - \frac{(G/G_{max} - 0.5)^2}{\exp(3.62)}} \tag{2.22}$$

This model results in small σ_{NG} when G/G_{max} is close to 1 or 0 and relatively large σ_{NG} when G/G_{max} is equal to 0.5. The standard deviation of the damping ratio (σ_D) is computed by:

$$\sigma_D = \exp(-5.0) + \exp(-0.25)\sqrt{D(\%)} \tag{2.23}$$

In the damping ratio model, the σ_D increases with increasing damping ratio. Using these definitions for the standard deviation, the $\pm\sigma$ modulus reduction and damping curve for sand at a confining pressure of 1 atm are shown in Figure 2.9.

2.2 Site Response Methods

The previous section introduced transfer functions which transform the input Fourier amplitude spectrum (FAS) into a FAS of strain, acceleration, and even a single-degree-of-freedom oscillator at any depth within the site profile. In both the time domain and random vibration theory methods, the same transfer functions are applied to the input FAS. The difference in the methods is in how this FAS in the frequency domain is converted into the time domain information.

2.2.1 Time Series Method

In the time series method, an input acceleration-time history is provided and the input FAS is computed from that time series using the fast Fourier transform (FFT) to compute the discrete Fourier transformation on the provided time series. The computed FAS is complex valued, and can be converted into amplitude and phase information. Strata uses the free and open-source FFTW library (`http://www.fftw.org`). The inverse discrete Fourier transform is used to compute a time series for a given FAS. The details of the FFT process are not discussed here, but can be found on the FFTW webpage.

In Strata, the time series is padded with zeros to obtain a number of points that is a power of two. If a time series contains a power of two values, then it is padded with zeros until the next power of two.

The frequencies associated with the FAS are computed from the time step between points and the number of points (N) in the record. The highest possible sampling frequency is known as the Nyquist frequency and is defined as:

$$f_{Nyquist} = \frac{1}{2\Delta t} \tag{2.24}$$

where Δt is the time increment between data points. The increment between the frequencies is calculated by:

$$\Delta f = \frac{f_{Nyquist}}{N/2 - 1} = \frac{1}{2\Delta t\,(N/2 - 1)} \tag{2.25}$$

After the FAS of the motion has been computed it is possible to perform site response analysis with the motion. The following is a summary of the steps to compute the surface acceleration time-series for the site described in Table 2.1:

1. Read the acceleration-time series file (Figure 2.10a).

2. Compute the input FAS with the Fast Fourier transformation (FFT) (Figure 2.10b, only amplitude is shown).

3. Compute the transfer function for the site properties (Figure 2.10c, only amplitude is shown).

4. Compute the surface FAS by applying the transfer function to the input FAS (Figure 2.10d, only amplitude is shown).

5. Compute the surface acceleration-time series through the inverse FFT of the surface FAS (Figure 2.10e).

2.2.2 Random Vibration Theory Method

The random vibration theory (RVT) approach to site response analysis was first proposed in the engineering seismology literature (e.g. Schneider et al. (1991)) and has been applied to site response analysis (Rathje et al., 2005; Silva et al., 1997). RVT does not utilize time domain input motions, but rather initiates all computtions with the input FAS (amplitude only, no phase information). Because RVT does not have the accompanying phase angles to the Fourier amplitudes, a time history of motion cannot be computed. Instead, extreme value statistics are used to compute peak time domain parameters of motion (e.g. peak ground acceleration, spectral acceleration) from the Fourier amplitude information. Due to RVT's stochastic nature one analysis can provide a median estimate of the site response with a single analysis and with the need for time domain input motions.

The Basics of RVT

Random vibration theory can be separated into two parts: (1) conversion between time and frequency domain using Parseval's theorem, and (2) estimation of the peak factor using extreme value statistics.

Consider a time varying signal $x(t)$ with its associated Fourier amplitude spectrum, $X(f)$. The root-mean-squared value of the signal (x_{rms}) is a measure of its average value over a given time period, T_{rms}, and is computed from the integral of the times series over that time period:

$$x_{rms} = \sqrt{\frac{1}{T_{rms}} \int_0^{T_{rms}} [x(t)]^2 \, \mathrm{d}t} \tag{2.26}$$

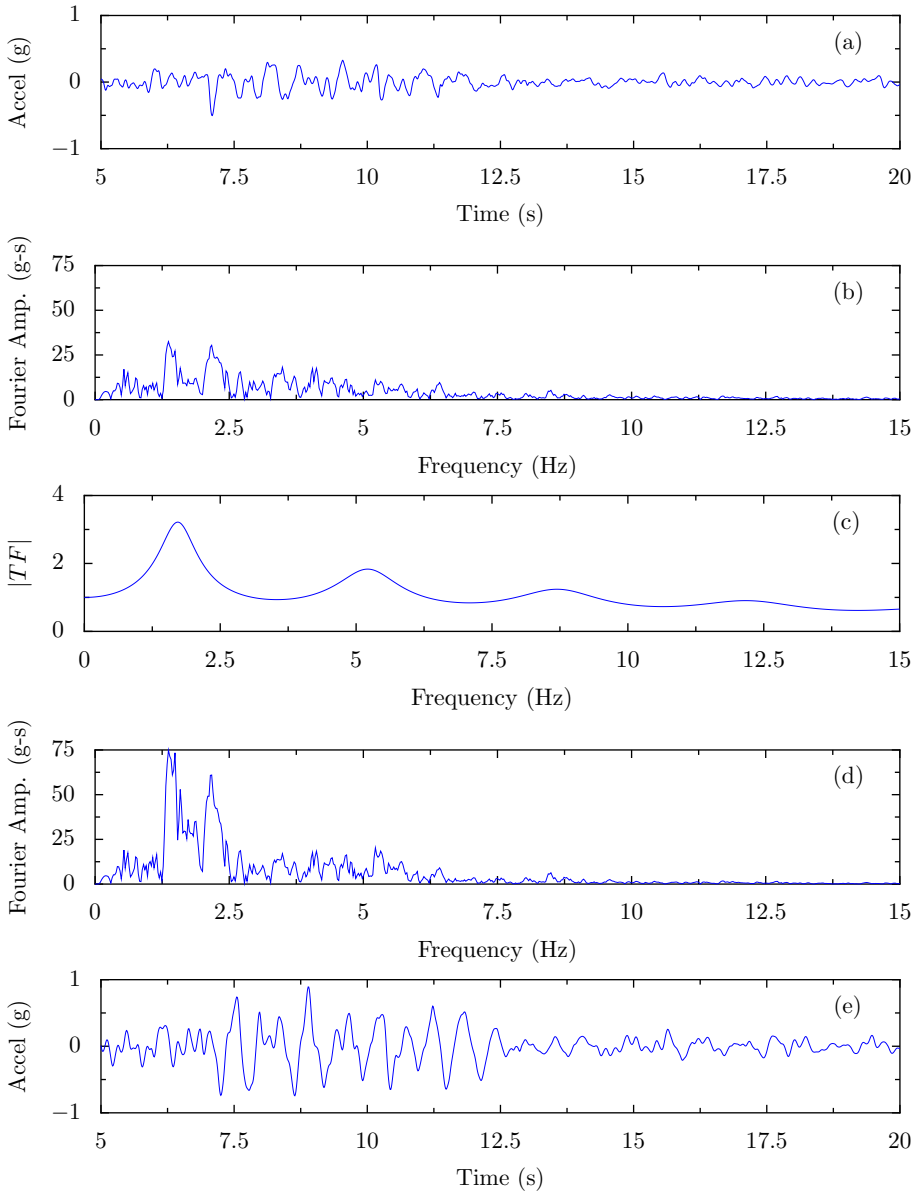

Figure 2.10: Time domain method sequence: (a) input acceleration-time series, (b) input Fourier amplitude spectrum, (c) transfer function from input to surface, (d) surface Fourier amplitude spectrum, and (e) surface acceleration-time series.

Parseval's theorem related the integral of the time series to the integral of its Fourier Transform, such that Equation 2.26 can be written in term of the FAS of the signal:

$$x_{rms} = \sqrt{\frac{2}{T_{rms}} \int_0^\infty |X(f)|^2 \, \mathrm{d}f} = \sqrt{\frac{m_0}{T_{rms}}} \tag{2.27}$$

where m_0 is defined as the zero-th moment of the FAS. The n-th moment of the FAS is defined as:

$$m_n = 2 \int_0^\infty (2\pi f)^n \, |X(f)|^2 \, \mathrm{d}f \tag{2.28}$$

The peak factor (PF) represents the ratio of the maximum value of the signal (x_{max}) to its *rms* value (x_{rms}), such that if x_{rms} and PF are known, then x_{max} can be computed using:

$$x_{max} = PF \cdot x_{rms} \tag{2.29}$$

Cartwright and Longuet-Higgins (1956) studied the statistics of ocean wave amplitudes, and considered the probability distribution of the maxima of a signal to develop expressions for the PF in terms of the characteristics of the signal. Cartwright and Longuet-Higgins (1956) derived an integral expression for the expected values of the peak factor in terms of the number of extrema (N_e) and the bandwidth (ξ) of the time series (Boore, 2003):

$$E[PF] = \sqrt{2} \int_0^\infty 1 - \left[1 - \xi \exp\left(-z^2\right)\right]^{N_e} \, \mathrm{d}z \tag{2.30}$$

where the bandwidth is defined as:

$$\xi = \sqrt{\frac{m_2^2}{m_0 m_4}} \tag{2.31}$$

and the number of extrema is defined as:

$$N_e = \frac{1}{\pi} \sqrt{\frac{m_4}{m_2}} T_{gm} \tag{2.32}$$

Boore and Joyner (1984) illustrated the need to modify the duration used in the *rms* calculation when considering oscillator responses, and they introduced the concept of an *rms* duration (T_{rms}). The *rms* duration requires

modification for spectral acceleration to account for the enhanced duration due to the oscillator response. Generally, adding the oscillator duration to the ground motion duration will suffice, except in cases where the ground motion duration is short (Boore and Joyner, 1984). Boore and Joyner (1984) recommend the following expressions to define T_{rms}:

$$T_{rms} = T_{gm} + T_o \left(\frac{\gamma^n}{\gamma^n + \alpha} \right) \tag{2.33}$$

$$\gamma = \frac{T_{gm}}{T_n} \tag{2.34}$$

$$T_o = \frac{T_n}{2\pi\beta} \tag{2.35}$$

where T_o is the oscillator duration, T_n is the oscillator natural period, and β is the damping ratio of the oscillator. Based on numerical simulations, Boore and Joyner (1984) proposed $n = 3$ and $\alpha = \frac{1}{3}$ for the coefficients in Equation 2.33.

Defining the Input Motion

The input motion in an RVT analysis is defined by a ground motion duration (T_{gm}) and a Fourier amplitude spectrum (FAS). The FAS can be directly computed using seismological source theory (e.g (e.g. Brune, 1970, 1971)), or it can be back-calculated from an acceleration response spectrum (see section 2.2.2 on page 20). Strata does not provide implementation for any seismological source theory models but does allow for the Fourier amplitude spectrum to be directly provided. The frequencies provided with the Fourier amplitude spectrum is the frequency range used by the program so it is critical that enough points be provided.

Calculation of the duration for use in RVT analysis can be done using seismological source theory or empirical models. Boore (2003) recommends the following description of ground motion duration (T_{gm}) for the Western United States:

$$T_{gm} = \underbrace{\frac{1}{f_0}}_{\text{Source duration, } T_s} + \underbrace{0.05R}_{\text{Path duration, } T_p} \tag{2.36}$$

where R is the distance in km, and the corner frequency (f_o) in hertz is given by:

$$f_0 = 4.9 \cdot 10^6 \beta_s \left(\frac{\Delta\sigma}{M_0} \right)^{1/3}$$

where $\Delta\sigma$ is the stress drop in bar, β_s is the shear-wave velocity in units of km/s, and M_0 is the seismic moment is units of dyne-cm (Brune, 1970, 1971). The seismic moment (M_0) is related to the moment magnitude (M_w) by:

$$M_0 = 10^{\frac{3}{2}(M_0+10.7)}$$

For the Eastern United States, Campbell (2003) proposes that the path duration effect be distance dependent:

$$T_p = \begin{cases} 0 & R \leq 10\text{km} \\ 0.16R & 10\text{km} < R \leq 70\text{km} \\ -0.03R & 70\text{km} < R \leq 130\text{km} \\ 0.04R & R > 130\text{km} \end{cases} \tag{2.37}$$

Empirical ground motions duration models (e.g. Abrahamson and Silva, 1996) can also be used to estimate the duration of the scenario event (T_{gm}). When such a model is applied, it is recommended that T_{gm} be taken as time between the build up from 5% to 75% of the normalized arias intensity (D_{5-75}).

Calculation of a FAS from an Acceleration Response Spectrum

The input rock FAS ($Y(f)$) can be derived from an acceleration response spectrum using an inverse technique. The inversion technique follows the basic methodology proposed by Gasparini and Vanmarcke (1976) and further described by Rathje et al. (2005). The inversion technique makes use of the properties of the single-degree-of-freedom (SDOF) transfer function used to compute the response spectral values. The square of the Fourier amplitude at the SDOF oscillator natural frequency f_n ($|Y(f_n)|^2$) can be written in terms of the spectral acceleration at f_n (S_{a,f_n}), the peak factor (PF), *rms* duration of the motion (T_{rms}), the square of the Fourier amplitudes ($|Y(f)|^2$) at frequencies less than the natural frequency, and the integral of the SDOF transfer function ($|H_{f_n}(f)|^2$):

$$|Y(f_n)|^2 \approx \frac{1}{\int_0^\infty |H_{f_n}(f)|^2 \, \mathrm{d}f - f_n} \left(\frac{T_{rms}}{2} \frac{S_{a,f_n}^2}{PF^2} - \int_0^{f_n} |Y(f)|^2 \, \mathrm{d}f \right) \tag{2.38}$$

Within Equation 2.38, the integral of the transfer function is constant for a given natural frequency and damping ratio (β), allowing the equation to be simplified to (Gasparini and Vanmarcke, 1976):

$$|Y(f_n)|^2 \approx \frac{1}{f_n \left(\frac{\pi}{4\beta} - 1 \right)} \left(\frac{T_{rms}}{2} \frac{S_{a,f_n}^2}{PF^2} - \int_0^{f_n} |Y(f)|^2 \, \mathrm{d}f \right) \tag{2.39}$$

The peak factors in Equation 2.39 depend on the moments of the FAS which is currently undefined. So the peak factors for all natural frequencies are initially assumed to be 2.5. Equation 2.39 is applied first to the spectral acceleration of the lowest frequency (longest period) provided by the user. At this frequency, the FAS integral term in Equation 2.39 can be assumed to be equal to zero. The equation is then applied at successively higher frequencies using the previously computed values of $|Y(f)|$ to assess the integral.

After an initial estimate of the FAS is developed using Equation 2.39 with assumed constant peak factors, it would be possible to recompute the peak factors for each period. The variable peak factors would provide a better estimate of the FAS from the target response spectrum. This approach was originally implemented, but the FAS based on the variable peak factors still resulted in a response spectrum that was more than 10% different than the target response spectrum at short periods.

To improve the agreement between the RVT-derived FAS (and associated response spectrum) and the target response spectrum by correcting the FAS by the ratio of the two response spectra. This correction technique is possible because of the narrow band property of the SDOF transfer function. Using an iterative process, the FAS from iteration i is corrected by the ratio of the spectral acceleration computed by RVT ($S_a^{\text{RVT}}(f)$) to the target ($S_a^{\text{target}}(f)$) at each frequency:

$$|Y_{i+1}(f)| = \frac{S_a^{\text{RVT}}(f)}{S_a^{\text{target}}(f)}|Y_{i+1}(f)| \tag{2.40}$$

The following process is used in the generate a corrected FAS:

1. Initial FAS is computed using the Vanmarcke (1983) technique.
2. The acceleration response spectrum associated with this FAS is computed using RVT.
3. The FAS is corrected using equation (2.40).
4. Using the corrected FAS, a new acceleration response spectrum is calculated.

This process is repeated with three conditions:

1. maximum of 30 iterations,
2. a root-mean-square-error of 0.005 is achieved, or

3. the change in the root-mean-square-error is less than 0.001.

This ratio correction works very well in producing a FAS that agrees with the target response spectrum, but the resulting FAS may have an inappropriate shape at some frequencies, as discussed below.

To demonstrate the inversion process consider a scenario event of a magnitude 6.5 earthquake with a strike-slip faulting mechanism at a distance of 20 km. The target response spectrum is computed using the Abrahamson and Silva (1997) attenuation model (Figure 2.11). An initial estimate of the FAS is computed using the Gasparini and Vanmarcke (1976) method and then the ratio correction algorithm is applied. This methodology results in a good agreement – less than 5% relative error as shown in Figure 2.13 – with the target response spectrum (Figure 2.11), but the associated FAS tends to curl up at low and high frequencies (curve labeled "Ratio Corrected" in Figure 2.12). The curling up at low frequencies can be mitigated by extending the frequency domain.

The frequency domain is extended to half of the minimum frequency and twice the maximum frequency specified in the target response spectrum. For example, if the target response spectrum is provided from 0.2 to 100 Hz (5 to 0.01 seconds), then the frequencies of the FAS are defined to be 2048 points equally spaced in log space from 0.1 to 200 Hz. The resulting response spectrum shows even better agreement with a maximum error of about 3% (curve labeled "Ratio and Extrapolated" in Figure 2.13).

Theoretically the slope of the FAS at high frequencies should be increasingly negative due to a path-independent loss of the high-frequency motion (Boore, 2003). However, in the computed FAS the slope actually increases at around 50 Hz (Figure 2.12). At first glance it may not appear that this relatively small amount of high frequency energy is important. However, in site response analysis the damping in the soil further attenuates this high frequency portion of the FAS, and the peak factor depends on the 4^{th} moment which is sensitive to this high frequency energy. The result is that the strain (or acceleration) near the surface – after attenuation of the high frequency energy has occurred – is significantly less than it computed using traditional time domain methods. To solve for this shortcoming, the slope of the FAS at high frequencies is forced down (Figure 2.12). However, this solution results in a slight under prediction of the peak ground acceleration (Figure 2.11 and 2.13).

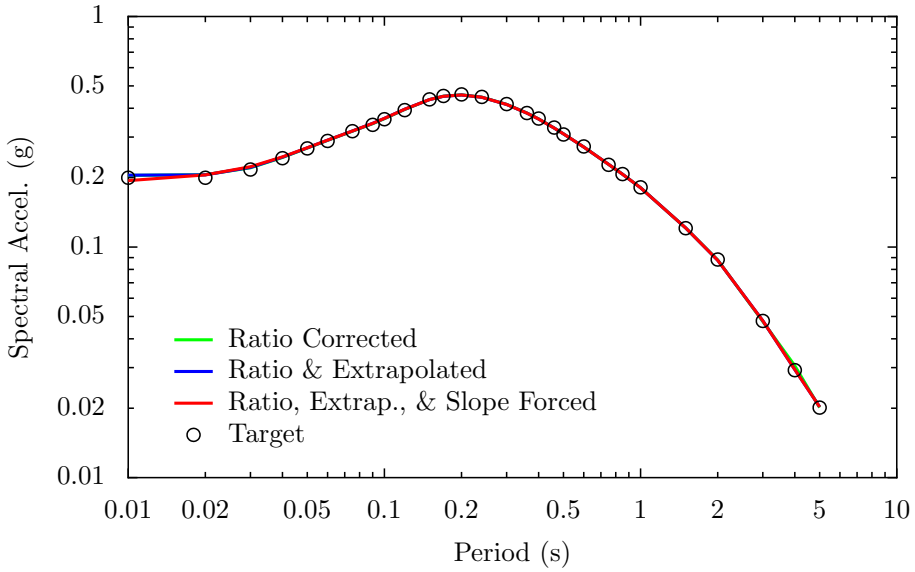

Figure 2.11: The comparison between the target response spectrum and the response spectrum computed with RVT.

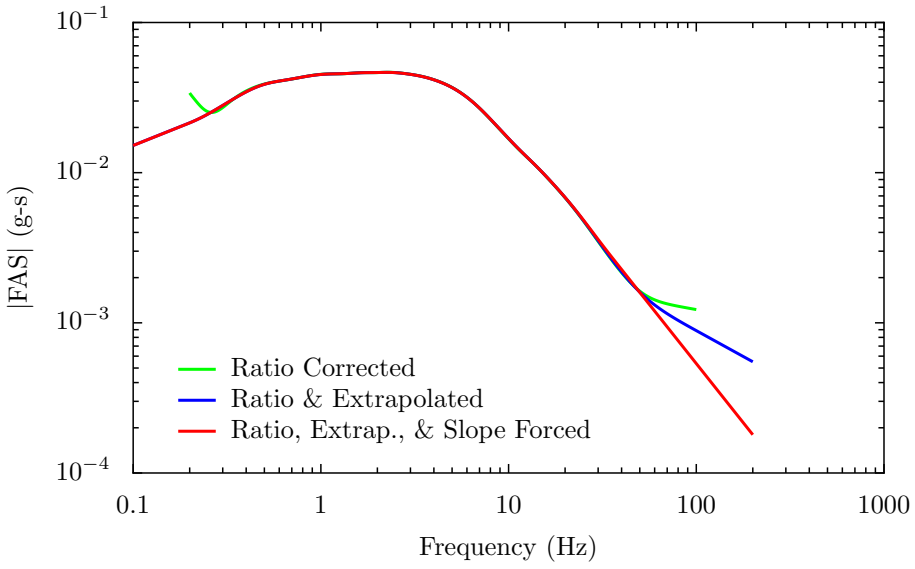

Figure 2.12: The FAS computing through the inversion process.

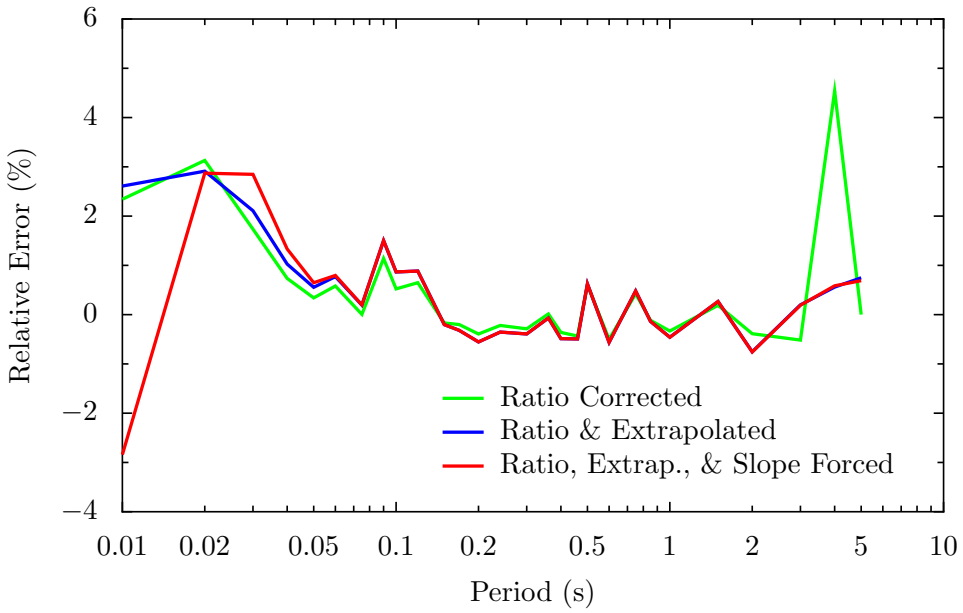

Figure 2.13: The relative error between the computed response spectra and the target response spectrum.

Example of the RVT Procedure

The following is an example of the random vibration theory based site response analysis to estimate the peak acceleration at the top of the site described in Table 2.1: The earthquake scenario is a magnitude 6.5 event at a distance of 20 km, as described in the previous section.

1. Empirical relationships are used to specify the input rock response spectrum (Figure 2.11) and ground motion duration ($T_{gm} = D_{5-75}$ =4.55s).

2. Using the inversion technique, the FAS corresponding to the target response spectrum is computed (Figure 2.14a). In this example, the maximum acceleration of the input motion is computed with RVT to allow for a comparison in the peak response between the surface and the input. The RVT calculation results are shown in Table 2.2.

Parameter	**Input Motion Value**	**Equation**
Moments of FAS (m_0, m_2, and m_4)	0.0280, 93.8435, and $1.7382 \cdot 10^7$	2.28
Bandwidth (ξ)	0.1346	2.31
Number of extrema (N_e)	623.3158	2.32
Peak factor (PF)	3.1406	2.30
Root-mean-square acceleration (a_{rms})	0.0784 g	2.27
Expected maximum acceleration (a_{max})	0.2462 g	2.29

Table 2.2: The values of the RVT calculation for the input motion.

3. Compute the transfer function for the site properties (Figure 2.14b).

4. Compute the surface FAS by applying the absolute value of the transfer function to the input FAS (Figure 2.14c). Using the surface FAS the maximum expected acceleration can be computed as presented in Table 2.3. The calculation shows that the site response increases the expected peak ground acceleration by approximately 34%.

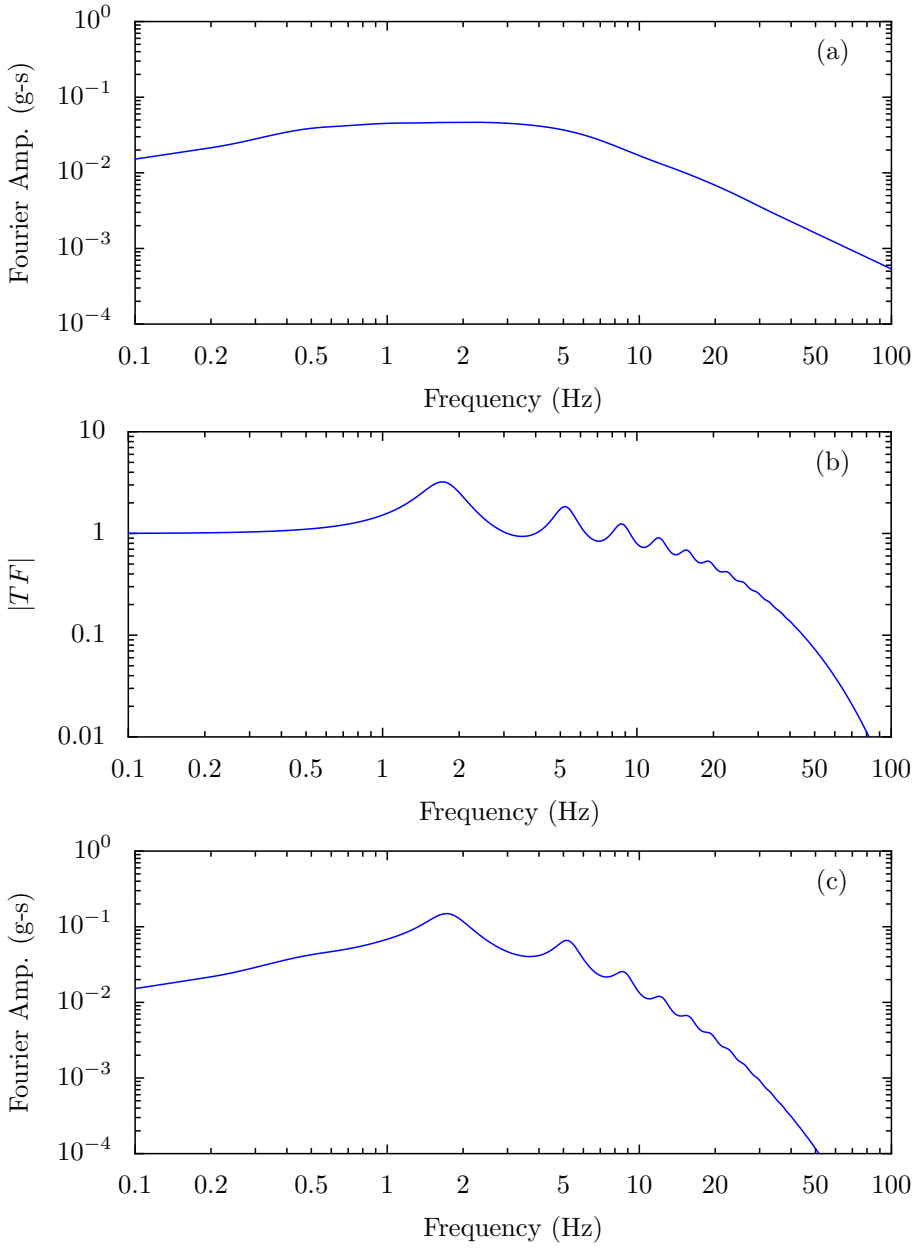

Figure 2.14: Random vibration theory method sequence: (a) input Fourier amplitude spectrum, (b) transfer function from input to surface, and (c) surface Fourier amplitude spectrum.

Parameter	Value		Equation
	Input Motion	**Surface Motion**	
Moments of FAS (m_0, m_2, and m_4)	0.0280, 93.8435, and $1.7382 \cdot 10^7$	0.0635, 39.6356, and $1.6306 \cdot 10^5$	2.28
Bandwidth (ξ)	0.1346	0.3895	2.31
Number of extrema (N_e)	623.3158	92.8944	2.32
Peak factor (PF)	3.1406	2.8568	2.30
Root-mean-square acceleration (a_{rms})	0.0784 g	0.1181 g	2.27
Expected maximum acceleration (a_{max})	0.2462 g	0.3375 g	2.29

Table 2.3: The values of the RVT calculation for the input and surface motions.

Chapter 3

Variation of Site Properties

3.1 Introduction

A soil profile consists of discrete layers that vary in thickness based on the properties of the soil. The layers are typically discretized based on the soil type, recorded from borehole samples or inferred from a shear-wave velocity profile. In seismic site response analysis, each layer is characterized by a thickness, mass density, shear-wave velocity, and nonlinear properties (G/G_{max}, and D). One of the challenges in defining values for these properties is the natural variability across a site and the uncertainty in their measurement. Because the dynamic response of a site is dependent on the soil properties, any variation in the soil properties will change both the expected surface motion and its standard deviation.

In a simple system, the variability of the components can be analytically combined to quantify the variability of the complete system, thus allowing for the expected value and variability of the system response to be computed. In seismic site response analysis, the nonlinear response of the system does not allow an exact analytic quantification of the variability of the site response. Instead, an estimate of the expected surface response and its standard deviation due to variations in the soil properties can be made through Monte Carlo simulations. Monte Carlo simulations estimate the response of a system by generating parameters of the system based on defined statistical distributions and computing the response for each set of input parameters. The following chapter introduces Monte Carlo simulations as applied to site response analysis and presents the models that describe the variability of the layering, shear-wave velocity, and nonlinear properties (G/G_{max} and D).

3.2 Random Variables

The goal of a Monte Carlo simulation is to estimate the statistical properties of the response of a complex system. To achieve this goal, each of the properties of the system is selected from defined statistical distributions and the response of the system is computed. The response is computed for many realizations and the calculated response from each realization is then used to estimate statistical properties of the system's response. While Monte Carlo simulations can be used on a wide variety of problems, a major disadvantage is that a large number of simulations is required to achieve stable results.

Monte Carlo simulations require that each of the components in the system has a complete statistical description. The description can be in the form of a variety of statistical distributions (i.e. uniform, triangular, normal, log-normal, exponential, etc.), however the normal and log-normal distributions typically are used because they can be easily described using a mean (μ) and standard deviation (σ). For normally distributed variables, a random value (x) can be generated by:

$$x = \sigma_x \cdot \varepsilon + \mu_x \tag{3.1}$$

where μ_x is the mean value, σ_x is the standard deviation, and ε is a random variable with zero mean and unit standard deviation.

There are a variety of methods for generating random variables for a given distribution. The most general technique involves using the cumulative density function (CDF) to convert between probability and value. For example, the calculation of a normally distributed random variable is achieved by first calculating a random variable from a uniform distribution between 0 and 1. The random variable (ε) is then calculated by finding the inverse to this random value on the standard (σ=1) normal CDF, shown in Figure 3.1. If the distribution of the variable is not normal, a similar technique of using a random value from a unit uniform distribution and the CDF of the probability distribution of the variable can be used (Ang and Tang, 1990). While this method is applicable for a set of independent random variables, it may not be used when the variables are related (i.e. correlated).

In the case of random variables that are not independent, a more complicated procedure is required for the generation of values. Before discussing the technique for generating correlated random variables, the concepts of correlation and linear functions of random variables must be introduced.

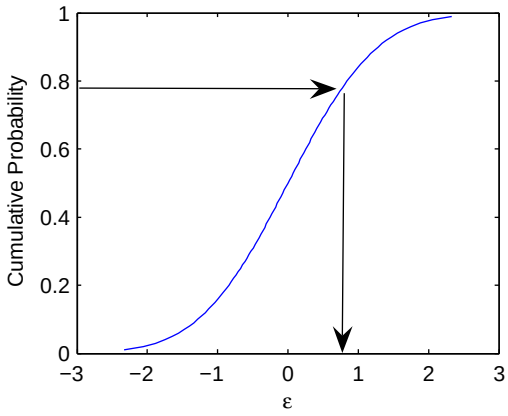

Figure 3.1: Using a random variable from a uniform distribution between 0 and 1 to generate a variable from a distribution with a zero mean and unit standard deviation.

Consider random variables x_1 and x_2. The covariance of the two random variables is defined as:

$$\text{cov}(x_1, x_2) = E[(x_1 - \mu_{x_1})(x_2 - \mu_{x_2})] = E[x_1 x_2] - E[x_1]E[x_2] \tag{3.2}$$

where E is the expected value and μ_{x_1} and μ_{x_2} are the mean values of x_1 and x_2, respectively (Ang and Tang, 1975). The covariance quantifies the strength of relationship between x_1 and x_2. If the variables are independent of each other (Figure 3.2a), then the covariance is zero, however a covariance of zero does not necessarily indicate the variables are independent. Instead, it indicates that the variables do not have a linear dependence. As the covariance becomes more positive, two variables have a greater tendency to both differ from their respective mean values in the same direction (Figure 3.2b). Conversely, as the covariance becomes more negative, variables have a greater tendency to differ in the opposite direction (Figure 3.2c). The covariance matrix ([C]) of a set of random variables is defined as:

$$[C]_{i,j} = \text{cov}(X_i, X_j) \tag{3.3}$$

For two variables, the covariance matrix expands to:

$$[C] = \begin{bmatrix} \text{cov}(x_1, x_1) & \text{cov}(x_1, x_2) \\ \text{cov}(x_2, x_1) & \text{cov}(x_2, x_2) \end{bmatrix} = \begin{bmatrix} \sigma_{x_1}^2 & \rho_{x_1,x_2}\sigma_{x_1}\sigma_{x_2} \\ \rho_{x_1,x_2}\sigma_{x_1}\sigma_{x_2} & \sigma_{x_2}^2 \end{bmatrix} \tag{3.4}$$

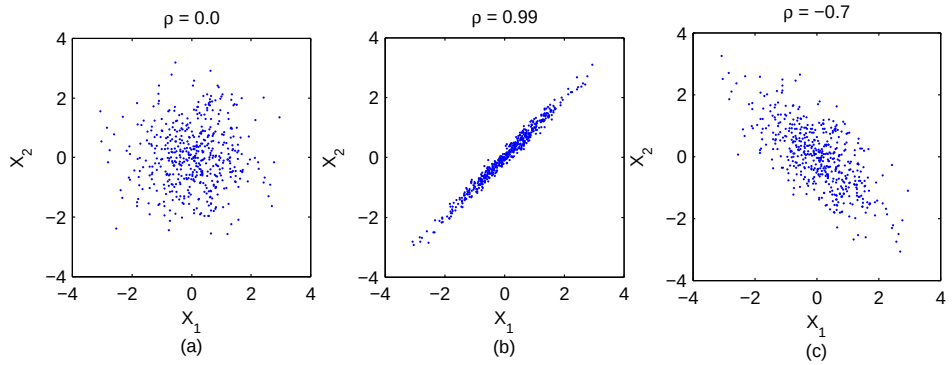

Figure 3.2: Two variables with a correlation coefficient of: (a) 0.0, (b), 0.99, and (c) -0.7.

where σ_{x_1} and σ_{x_2} are the standard deviations of x_1 and x_2, respectively, and ρ_{x_1,x_2} is the correlation coefficient, defined as:

$$\rho_{x_1,x_2} = \frac{\text{cov}(x_1, x_2)}{\sigma_{x_1}\sigma_{x_2}} = \frac{E[x_1x_2] - E[x_1]E[x_2]}{\sigma_{x_1}\sigma_{x_2}} \tag{3.5}$$

The correlation coefficient can range -1 to 1.

Independent random variables from a normal distribution are generated using equation (3.1) independently for each random variable. By combining the multiple applications equation (3.1) into a system of equations, the generation of two independent variables is achieved by multiplying a vector of random variables ($\vec{\varepsilon}$) by a matrix ($[\sigma]$) and adding a constant ($\vec{\mu}$), defined as:

$$\left\{ \begin{array}{c} x_1 \\ x_2 \end{array} \right\} = \left[\begin{array}{cc} \sigma_{x_1} & 0 \\ 0 & \sigma_{x_2} \end{array} \right] \left\{ \begin{array}{c} \varepsilon_1 \\ \varepsilon_2 \end{array} \right\} + \left\{ \begin{array}{c} \mu_1 \\ \mu_2 \end{array} \right\} \tag{3.6}$$

where ε_1 and ε_2 are random variables randomly selected from a standard normal distribution ($\mu = 0$ and $\sigma = 1$), σ_{x_1} and σ_{x_2} are the standard deviations of x_1 and x_2, respectively, and μ_{x_1} and μ_{x_2} are the mean values of x_1 and x_2, respectively. Because the random variables x_1 and x_2 are independent ($\rho_{x_1,x_2} = 0$), the off-diagonal values in the matrix ($[\sigma]$) are zero.

Using the same framework, a linear system of equations is used to generate a pair of correlated random variables. However, because of the correlation between x_1 and x_2 the off diagonal values in the matrix will no longer be zero. Instead, a pair of correlated random variables ($\vec{x}$) are

generated by:

$$\left\{ \begin{array}{c} x_1 \\ x_2 \end{array} \right\} = \left[\begin{array}{cc} \sigma_{x_1} & 0 \\ \rho_{x_1,x_2}\sigma_{x_2} & \sigma_{x_2}\sqrt{1-\rho_{x_1,x_2}^2} \end{array} \right] \left\{ \begin{array}{c} \varepsilon_1 \\ \varepsilon_2 \end{array} \right\} + \left\{ \begin{array}{c} \mu_1 \\ \mu_2 \end{array} \right\} \tag{3.7}$$

Here, the first random variable (x_1) is calculated based on the value of ε_1 alone, while the second random variable (x_2) is a function of both ε_1 and ε_2. Note that ε_1 and ε_2 still represent random and independent variables generated from the standard normal distribution.

3.3 Statistical Models for Soil Properties

For the properties of the soil to be randomized and incorporated into Monte Carlo simulations, the statistical distribution and properties of the soil need to be characterized. In this research, two separate models are used. The first model, developed by Toro (1995), describes the statistical distribution and correlation between layering and shear-wave velocity. The second model by Darendeli (2001) was previously introduced in Section 2.1.3 and is used to describe the statistical distribution of the nonlinear properties (G/G_{max} and D).

3.3.1 Layering and Velocity Model

In Strata, the randomization of the layering and the shear-wave velocity is done through the use of the velocity profile model proposed by Toro (1995). The Toro (1995) models provides a framework for generating layering and then to vary the shear-wave velocity of these layers. This model improves upon previous work by quantifying the correlation between the velocities in adjacent layers. In previous models, one of two assumptions were made that simplified the problem: the velocities at all depths were perfectly correlated and could be randomized by applying a constant random factor to all velocities (McGuire et al., 1989; Toro et al., 1992), or the velocities within each of the layers are independent of each other, and therefore can be randomized by applying an independent random factor to each layer (Costantino et al., 1991). While these two assumptions simplify the problem, they represent two extreme conditions. The Toro (1995) model makes neither of these assumptions, instead the model incorporates a correlation between layers.

Layering Model

The layering is modeled as a Poisson process, which is a stochastic process with events occuring at a given rate (λ). For a homogeneous Poisson process this rate is constant, while for a non-homogeneous Poisson process the rate varies. Generally, a Poisson process models the occurrence of events over time, but for the layering problem the event is a layer interface and its rate is defined in terms of length (i.e., number of layer interfaces per meter).

In the Toro (1995) model, the layering thickness is modeled as non-homogeneous Poisson process where the rate changes with depth ($\lambda(d)$, where d is depth). Before considering the non-homogeneous Poisson process, first consider the simpler homogeneous Poisson process with a constant rate. For a Poisson process with a constant occurrence rate (λ), the distance between layer boundaries, or layer thickness (h), is an exponential distribution with rate λ. The probability density function of an exponential distribution is defined as:

$$f(h;\lambda) = \begin{cases} \lambda \exp(-\lambda h) & \text{for } h \geq 0 \\ 0 & \text{for } h < 0 \end{cases} \tag{3.8}$$

The cumulative density function for the exponential distribution is given by:

$$F(h;\lambda) = \begin{cases} 1 - \exp(-\lambda h) & \text{for } h \geq 0 \\ 0 & \text{for } h < 0 \end{cases} \tag{3.9}$$

A random layer thickness with an exponential distribution is generated by solving Equation 3.9 with respect to thickness (t):

$$h = \frac{\ln\left[1 - F(h)\right]}{-\lambda} \quad \text{for } 0 < F(h) \leq 1 \tag{3.10}$$

By randomly generating probabilities ($F(t)$) with a uniform distribution and computing the associated thicknesses with Equation 3.10, a layering profile was simulated for 8 layers with a rate of 1 shown in Figure 3.3.

Simulating a non-homogeneous Poisson process is achieved by first simulating a homogeneous Poisson process and then warping the homogeneous layer boundaries (S'_n) into the non-homogeneous equivalent (S_n). The process is very similar to the generation of random variables with a specific distribution where a uniform distribution is warped into a particular distribution using the CDF. For a non-homogeneous Poisson process with rate $\lambda(d)$ the cumulative rate ($\Lambda(d)$) is defined as:

$$\Lambda(d) = \int_0^d \lambda(s)\,\mathrm{d}s \tag{3.11}$$

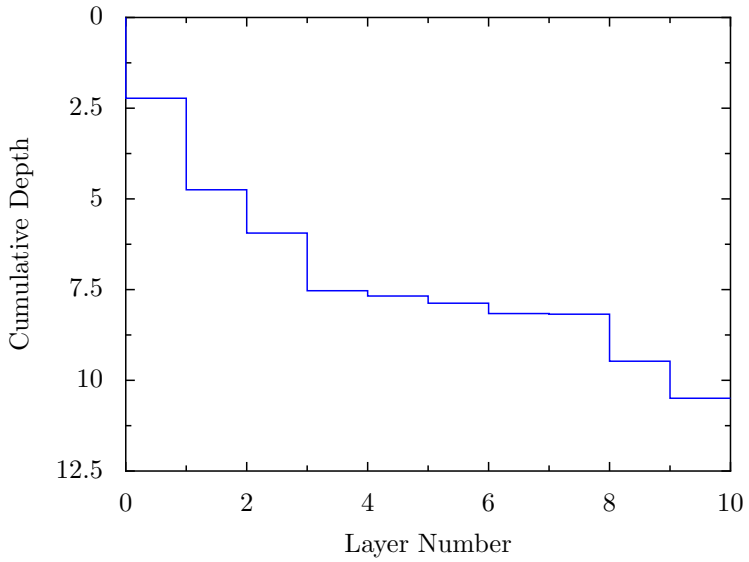

Figure 3.3: A layering profile consisting of 8 layers modeled by a homogeneous Poisson process with a rate of 1.

$\Lambda(d)$ represents the expected number of layers up to a depth d. The non-homogeneous process is simulated by generating exponential distributions with a unit rate ($\lambda = 1$) and mapping them to the non-homogeneous space using the inverse of Equation 3.11 ($\Lambda^{-1}(d)$).

As an example, the warping technique will be used on the homogeneous Poisson process to take a unit rate exponential random variables and convert them into a non-unit rate

Before $\Lambda^{-1}(d)$ can be defined, $\Lambda(d)$ and $\lambda(d)$ must be defined.

Toro (1995) proposed the following generic depth dependent rate model:

$$\lambda(d) = a \cdot (d + b)^c \tag{3.12}$$

The coefficients a, b, and c were estimated by Toro (1995) using the method of maximum likelihood applied to the layering measured at 557 sites, coming mostly from California. The resulting values of a be 1.98, 10.86, and -0.89, respectively. The occurrence rate ($\lambda(d)$) quickly decreases as the depth increases (Figure 3.4(a)). This decrease in the occurrence rate increases the expected thickness of deeper layers. The expected layer thickness (h) is equal to the inverse of the occurrence rate ($\lambda(d)$) and is shown in Figure 3.4(b).

The expected thickness ranges from 4.2 m at the surface to 59 m at a depth of 200 m.

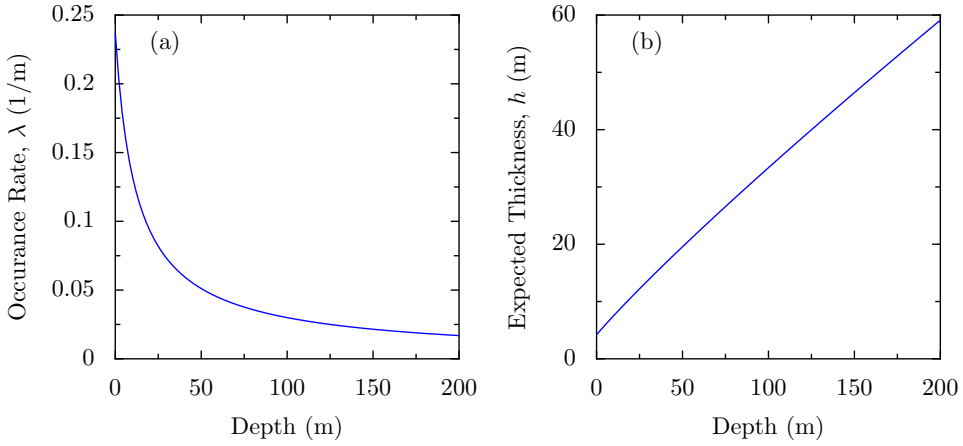

Figure 3.4: Toro (1995) layering model. (a) The occurrence rate (λ) as a function of depth (d), and (b) the expected layer thickness (h) as a function of depth.

Using Equations 3.11 and 3.12 the cumulative rate for the Toro (1995) modeled is defined as:

$$\Lambda(d) = \int_0^d a \cdot (s+b)^c \, \mathrm{d}s = a \cdot \left[\frac{(d+b)^{c+1}}{c+1} - \frac{b^{c+1}}{c+1} \right] \tag{3.13}$$

The inverse cumulative rate function is then defined as:

$$\Lambda^{-1}(d) = \left(\frac{c \cdot d}{a} + \frac{d}{a} + b^{c+1} \right)^{\frac{1}{c+1}} - b \tag{3.14}$$

Using this equation the homogeneous Poisson process (Figure 3.3) can be warped into a non-homogeneous Poisson process as shown in Figure 3.5. The resulting depth profile is shown in Figure 3.6.

Velocity Model

After the layering of the profile has been established, the shear-wave velocity profile can be generated. In the Toro (1995) model, the shear-wave

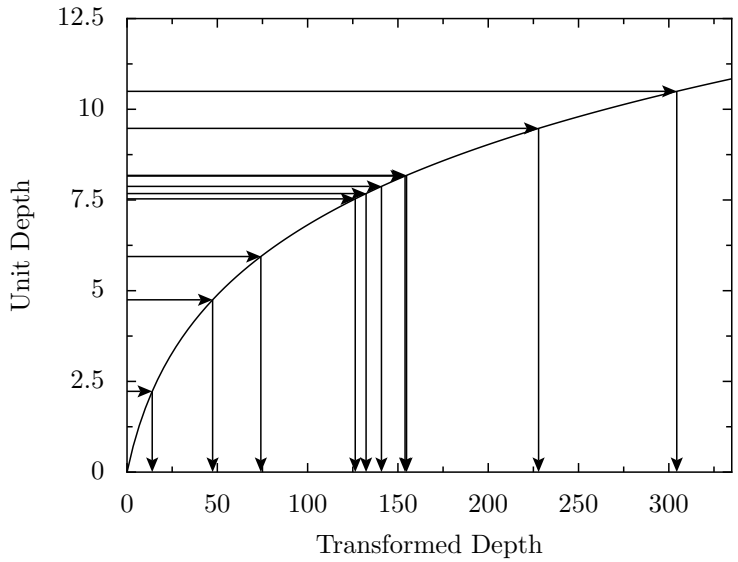

Figure 3.5: Transformation between a homogeneous Poisson process with rate 1 to the Toro (1995) non-homogeneous Poisson process.

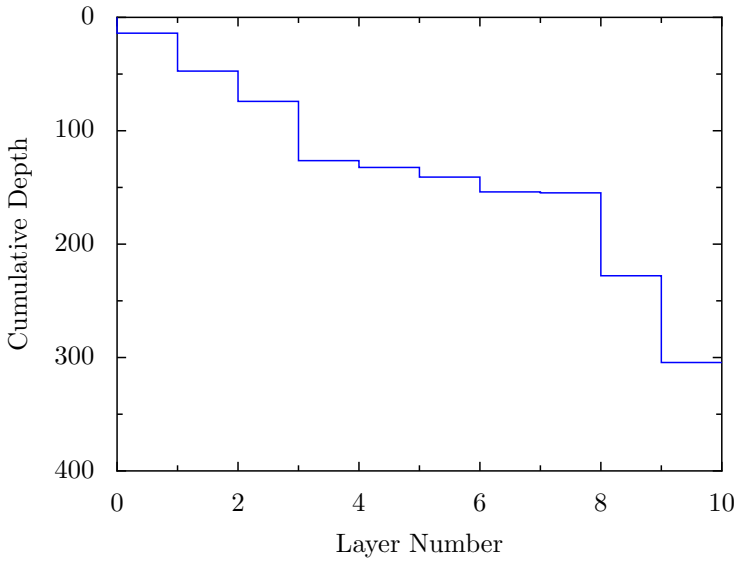

Figure 3.6: A layering simulated with the non-homogeneous Poisson process defined by Toro (1995).

velocity at mid-depth of the layer is described by a log-normal distribution. The standard normal variable (Z) of the i^{th} layer is calculated by:

$$Z_i = \frac{\ln(V_i) - \ln[V_{\text{median}}(d_i)]}{\sigma_{\ln\ V_s}} \tag{3.15}$$

where V_i is the shear-wave velocity in the i^{th} layer, $V_{\text{median}}(d_i)$ is the median shear-wave velocity at mid-depth of the layer and $\sigma_{\ln\ V_s}$ is the standard deviation of the natural logarithm of the shear-wave velocity. Equation 3.15 is then solved for the shear-wave velocity of the i^{th} layer (V_i):

$$V_i = \exp\{\sigma_{\ln\ V} \cdot Z_i + \ln[V_{median}(d_i)]\} \tag{3.16}$$

Equation 3.16 allows for the calculation of the velocity within a layer for a given median velocity at the mid-depth of the layer, standard deviation, and standard normal variable. In the model proposed by Toro (1995), values for median velocity versus depth ($V_{\text{median}}(d)$) and standard deviation ($\sigma_{\ln\ V_s}$) are provided based on site class. However, in the implementation of the Toro (1995) model in Strata the median shear-wave velocity is defined by the user. The standard normal variable of the i^{th} layer (Z_i) is correlated with the layer above it, and this inter-layer correlation is also dependent on the site class. The standard normal variable (Z_i) of the shear-wave velocity in the top layer ($i = 1$) is independent of all other layers and is defined as:

$$Z_1 = \varepsilon_1 \tag{3.17}$$

where ε_1 is an independent normal random variable with zero mean and a unit standard deviation. The standard normal variables of the other layers in the profile are calculated by a recursive formula, defined as:

$$Z_i = \rho \cdot Z_{i-1} + \varepsilon_i \cdot \sqrt{1 - \rho^2} \tag{3.18}$$

where Z_{i-1} is the standard normal variable of the previous layer, ε_i is a new normal random variable with zero mean and unit standard deviation, and ρ is the inter-layer correlation.

Correlation is a measure of the strength and direction of a relationship between two random variables. The inter-layer correlation between the shear-wave velocities proposed by Toro (1995) is a function of both the depth of the layer (d) and the thickness of the layer (h):

$$\rho(d, h) = [1 - \rho_d(d)] \cdot \rho_h(h) + \rho_d(d) \tag{3.19}$$

where ρ_h is the thickness dependent correlation and ρ_d is the depth dependent correlation. The thickness dependent correlation is defined as:

$$\rho_h(h) = \rho_0 \cdot \exp\left(\frac{-h}{\Delta}\right) \tag{3.20}$$

where ρ_0 is the initial correlation and Δ is a model fitting parameter. As the thickness of the layer increases, the thickness-dependent correlation decreases. The depth dependent correlation (ρ_d) is defined as a function of depth (d):

$$\rho_d(d) = \begin{cases} \rho_{200} \cdot \left[\frac{d+d_0}{200+d_0}\right]^b & \text{for } d \leq 200 \\ \rho_{200} & \text{for } d > 200 \end{cases} \tag{3.21}$$

where ρ_{200} is the correlation coefficient at 200 m and d_0 is an initial depth parameter. As the depth of the layer increases, the depth-dependent correlation increases. The final layer in a site response model is assumed to be infinitely thick, therefore the correlation between the last soil layer and the infinite half-space is only dependent on ρ_d. (Toro, 1995) evaluated each of the parameters in the correlation models ($\rho_0, \rho_{200}, \Delta, d_0, b$) for different generic site classes.

A site class is used to categorize a site based on the shear-wave velocity profile and/or local geology. In the Toro (1995) model, the statistical properties of the soil profile (the median velocity, standard deviation, and layer correlation) are provided for two different classifications schemes, the Geomatrix and USGS classifications. The Geomatrix site classification classifies sites based on a general description of the geotechnical subsurface conditions, distinguishing generally between rock, shallow soil, deep soil, and soft soil (Table 3.1). In contrast, the USGS site classification is based on the time-weighted average shear-wave velocity (see equation 2.9 of the top 30 meters ($\overline{v}_{s,30}$) (Table 3.2), and requires site specific measurements of shear-wave velocity.

Toro (1995) computed the statistical properties of the profiles for both the Geomatrix and USGS classifications using a maximum-likelihood procedure. The procedure used a total of 557 profiles, with 541 profiles for the USGS classification and only 164 profiles for the Geomatrix classification. The correlation parameters ($\rho_0, \rho_{200}, \Delta, d_0, b$) are presented in Table 3.3 and the median shear-wave velocities in are presented in Table 3.4.

Ten generated shear-wave velocity profiles were created for a deep, stiff alluvium site using the two previously discussed methods. In the first method, a generic site profile is generated by using the layering model

Designation	Description
A	Rock Instrument is found on rock material ($v_s > 600$ m/s) or a very thin veneer (less than 5 m) of soil overlying rock material.
B	Shallow (Stiff) Soil Instrument is founded in/on a soil profile up to 20 m thick overlying rock material, typically a narrow canyon, near a valley edge, or on a hillside.
C	Deep Narrow Soil Instrument is found in/on a soil profile at least 20 m thick overlying rock material in a narrow canyon or valley no more than several kilometers wide.
D	Deep Broad Soil Instrument is found in/on a soil profile at least 20 m thick overlaying rock material in a broad canyon or valley.
E	Soft Deep Soil Instrument is found in/on a deep soil profile that exhibits low average shear-wave velocity ($v_s < 150$ m/s).

Table 3.1: The categories of the geotechnical subsurface conditions (third letter) in the Geomatrix site classification (Toro, 1995).

Designation	Average Shear-Wave Velocity ($\overline{v}_{s,30}$)
A	greater than 750 m/s
B	360 to 750 m/s
C	180 to 360 m/s
D	less than 180 m/s

Table 3.2: The USGS site categories, where $\overline{v}_{s,30}$ is the time weighted average shear-velocity of the top 30 m (Toro, 1995).

	Site Classification							
	GeoMatrix		**USGS**					
Parameter	A & B	C & D	A & B	C & D	A	B	C	D
σ_{lnV}	0.46	0.38	0.35	0.36	0.36	0.27	0.31	0.37
ρ_0	0.96	0.99	0.95	0.99	0.95	0.97	0.99	0.00
ρ_{200}	0.96	1.00	1.00	1.00	0.42	1.00	0.98	0.50
Δ	13.1	8.0	4.2	3.9	3.4	3.8	3.9	5.0
d_0	0.0	0.0	0.0	0.0	0.0	0.0	0.0	0.0
b	0.095	0.160	0.138	0.293	0.063	0.293	0.344	0.744
Profiles	45	109	204	253	35	169	226	27
Layers	243	692	280	1487	129	750	1349	136

Table 3.3: Coefficients for the Toro (1995) model, calculated by maximum likelihood.

coefficients and median shear-wave velocity for a USGS C site class, shown in Figure 3.7(a). This approach essentially models the site as a generic USGS class C site, which is the general site classification of the for deep, stiff alluvium. The second method uses the layer correlation for the USGS C site class, but the layering and the median shear-wave velocity profile are defined from field measurements, shown in Figure 3.7(b). The site specific layering tends to be much thicker than the generic layering as a result of the field measurements indicating thick layers with the same shear wave velocity. In general both of the methods show an increase in the shear-wave velocity with depth. However, the site-specific shear-wave velocity values are significantly larger than the generic shear-wave velocity values. At the surface, the generic site has a median shear-wave velocity of 150 m/s compared to the site specific shear-wave velocity of 200 m/s. At a depth of 90 m, the difference is even greater, with the generic site having a median shear-wave velocity of 470 m/s compared to the site specific median shear-wave velocity of 690 m/s. The difference in shear-wave velocity is a result of the difference between the site specific information and the generic USGS site C median shear-wave velocity profile.

	Median Shear-Wave Velocity (m/s)							
	GeoMatrix		**USGS**					
Depth (m)	A & B	C & D	A & B	C & D	A	B	C	D
0.00	192	144	182	147	314	159	145	176
1.00	209	159	221	164	346	200	163	165
2.00	230	178	262	178	384	241	179	154
3.00	253	193	297	188	430	275	191	142
4.00	278	204	330	193	485	308	200	129
5.00	303	211	362	196	550	337	208	117
6.00	329	217	390	200	624	361	215	109
7.20	357	228	412	209	703	382	226	106
8.64	395	240	437	218	789	404	237	109
10.37	443	253	468	228	880	433	250	117
12.44	502	270	504	248	973	467	269	130
14.93	575	291	540	273	1070	501	291	148
17.92	657	319	578	296	1160	535	314	170
21.50	748	357	615	317	1260	567	336	192
25.80	825	402	653	347	1330	605	372	210
30.96	886	444	702	374	1380	654	391	229
37.15	942	474	734	386	1420	687	401	246
44.58	998	495	759	394	1460	711	408	266
53.20	1060	516	782	403	1500	732	413	289
64.20		541	805	427		749	433	318
77.04		566	834	459		772	459	353
92.44		593	870	488		802	486	392
110.93			922	515		847	513	435
133.12			983	550		900	550	
159.74				604			604	
191.69				682			676	
230.03				770			756	

Table 3.4: Median shear-wave velocity (m/s) based on the generic site classification.

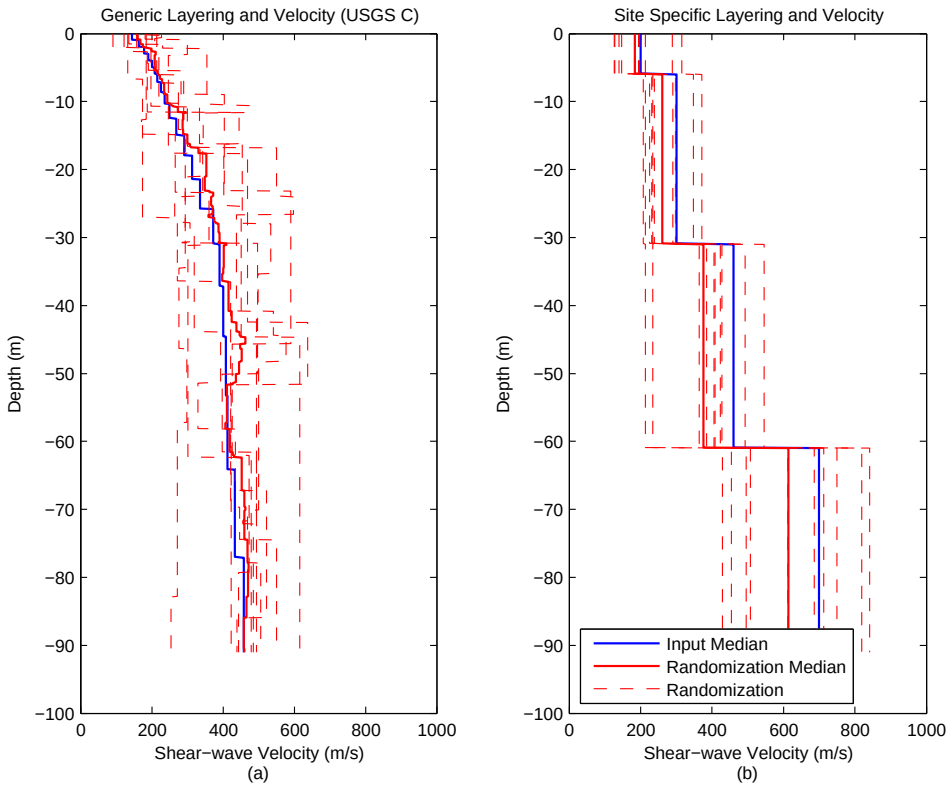

Figure 3.7: Ten generated shear-wave velocity (v_s) profiles for a USGS C site class. (a) Using generic layering and median v_s, (b) using user defined layering and median v_s.

3.3.2 Depth to Bedrock Model

...

3.3.3 Non-Linear Soil Properties Model

The Darendeli (2001) empirical model for nonlinear soil properties (G/G_{max} and D) was previously discussed in Section 2.1.3. The Darendeli (2001) empirical model assumes the variation of the properties is normal in distribution. The standard deviation of the G/G_{max} and the D varies with the magnitude of the property and is calculated with equations (2.22) and (2.23), respectively. Because the variation of the properties are modeled with a normal distribution is continuous from $-\infty$ to $+\infty$, the generated values of the shear-modulus reduction or damping ratio may fall below zero. The most likely location for the negative values occurs when the mean value is small, which occurs at large strains for the G/G_{max} and at low strains for D. Negative values for either G/G_{max} or D are not physically possible, therefore the normal distributions need to be truncated. To correct for this problem, minimum values for G/G_{max} and D are defined as 0.05 and 0.1%, respectively. These values were chosen as they represent appropriate minimum values. The influence of the minimum values on the site response results will be minimal because the truncation occurs only at the extremes of the strain range.

The G/G_{max} and D curves are not independent of each other. Consider a soil that behaves more linearly, that is to say the G/G_{max} is higher than the median G/G_{max}. During a loading cycle, the area inside the hysteresis would be smaller which is indicative of less damping within the system. As the linearity of the system increases, the damping decreases. To capture this effect, the soil properties are assumed to have a negative correlation with the default value set at -0.5 (i.e. $\rho = -0.5$). Using a correlation coefficient of -0.5, the nonlinear properties of sand (PI=0, OCR=0) at a confining pressure of 1 atm were generated 10 times, shown in Figure 3.8. Three of the realizations result in large shear modulus reduction curve relative to the mean. Because of the negative correlation, the relative high shear modulus reduction corresponds to a relative low damping ratio.

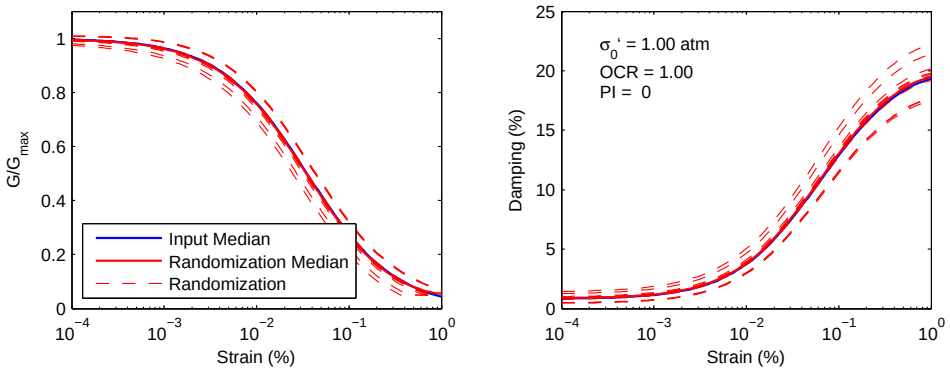

Figure 3.8: Generated nonlinear properties assuming perfect negative correlation.

Chapter 4

Using Strata

Strata is introduced through two examples that demonstrates the organization and most of the features found in Strata. Before these two examples some particular differences between Strata and other site response programs are introduced.

To someone that is used to working with text input files, operating Strata will seem a little foreign. With the exception of acceleration time-series, all of the input to Strata is entered via the keyboard, or through copying and pasting from spreadsheets. The input file is not saved in the typical text format, instead a binary format is used that is only readable by Strata. Furthermore, when the calculation is complete no output text files are produced. Instead, the output can be directly view with Strata and saved, once again to a binary format. There is the option for the data to be exported to text files that can then be opened with a variety of applications.

4.1 Strata Particulars

4.1.1 Auto-Discretization of Layers

One of the biggest differences between Strata and other site response analysis programs is the fact that the sublayers used in the calculation portion of the analysis are not defined by the user. Instead, the user defines a velocity layer that is then subdivided into sublayers by Strata. This fundamental difference exists because Strata allows for the layering and shear-wave velocity to vary (see Section 3.3.1 and therefore the required thickness of the sublayers changes.

The maximum thickness ($h_{\max}$) of the sublayers of i-th velocity layer

is take as a fraction of the minimum wavelength to be captured by the analysis:

$$h_{\max,i} = \lambda_{\text{frac}} \cdot \lambda_{\min} = \lambda_{\text{frac}} \cdot \frac{v_{s,i}}{f_{\max}} \tag{4.1}$$

where λ_{frac} is the wavelength fraction which typically varies between 1/10 and 1/5 (anything greater than 1/3 is not recommended), $f_{\max}$ is the maximum frequency of engineering interest which is typically around 20 Hz, and $V_{s,i}$ is the shear-wave velocity of the i-th layer. The actual thickness of the sublayers is less than the maximum thickness such that the velocity layer height divided by the sub-layer thickness is a whole number. These parameters are defined on the `General Settings` tab. To prevent the layers from being auto-discretized the wavelength fraction can be increased and the thickness velocity layers defined in the `Soil Profile` tab can be reduced to an appropriate level.

In other site response programs, the location of the input motion or the location of requested output (e.g., acceleration-time history) is generally referenced by a sublayer index. However, because the sublayers are computed in Strata (and may change for each realization), the location is defined in terms of the depth within the soil profile or at the top of the bedrock. When the location is specified as `Bedrock` then the actual depth of the location will change if the depth of the bedrock changes. The location is specified with a drop down list shown in Figure 4.1 where the user can specify the depth as `Bedrock` (Figure 4.1a) or a fixed depth (Figure 4.2c).

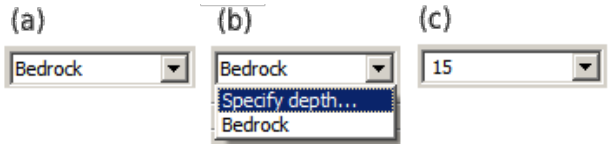

Figure 4.1: Location selection: (a) top of bedrock, (b) switching to a fixed depth, and (c) fixed depth of 15.

4.1.2 Interaction with Tables

For the majority of Strata, the input behaves as you would expect. The one exception may come when editing tables. Table cells are selected with one click. Once a cell is selected, the cell can be edited by typing. A cell's edit mode can be directly entered by double clicking on the cell. In some case

double clicking on a cell will produce a widget to aid specifying input to the cell.

All tables used in Strata are dynamic meaning the number of rows can be changed. Rows are added to the bottom on the list with the *Add* button. The *Insert* and *Remove* buttons are disabled until once a complete row has been selected, which is most easily achieved by clicking on the number next to the row of interest. Multiple continuous rows can be selected by pressing the *shift* key while selecting the rows. After rows have been selected: `Add` will add the same number of rows to the end of the table, `Insert` will insert the same number of rows to prior to the currently selected rows, and `Remove` will remove the selected rows. All rows in the table can be selected by click on the button in the upper right portion of the table as shown in Figure 4.2. Some table has cells that can not be edited and have a light gray background. An example of these cells is in the *Velocity Layers* table (shown Figure 4.2).

Data can copied from spreadsheets and be pasted into tables by:

1. Pressing `Ctrl+v`,
2. Clicking on the table, and then selecting `Paste` from the `Edit` menu, or
3. Right clicking on the table and selecting paste.

The table will automatically increase the numbers of rows to accommodate the size of the pasted data.

4.1.3 Non-Linear Curves

The nonlinear (shear-modulus reduction and damping) curves can be specified through three different methods in Strata: (1) fixed models that are present by default and cannot be removed, (2) user defined curves that can be used across projects, and (3) temporary models that only exist for the project.

Fixed Non-Linear Models

The following shear-modulus reduction models are included by default:

- Darendeli (2001)
- Iwasaki et al. (1976) – 0.25 and 1.0 atm

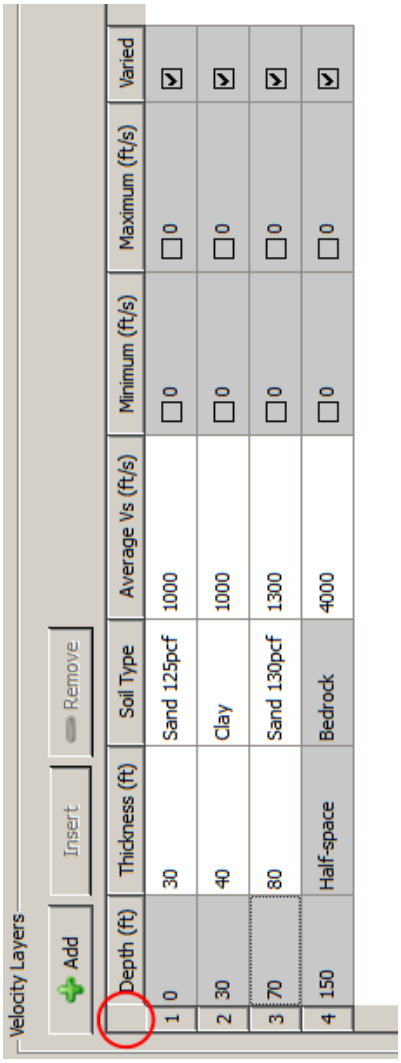

Figure 4.2: By clicking on the button circled in red all rows in the table are selected.

- Seed and Idriss (1970) – Mean and Upper
- Vucetic and Dobry (1991) – PI = 0, 15, 50, 100, and 200

and the following damping curves are included by default:

- Darendeli (2001)
- Seed and Idriss (1970) – Lower and Mean
- Vucetic and Dobry (1991) – PI = 0, 15, 50, 100, and 200

User Defined Models

Non-linear curve models can be defined for use across multiple projects by adding models to the library. The nonlinear property manager is opened by selecting `Add/Remove Non-Linear Property Curves` from the `Tools` menu. Using the dialog (Figure 4.3), a new model can be defined by following these steps:

1. Click the `Add` button to add a new curve to with the normalized shear-modulus reduction or damping models list.
2. Rename the model from "Untitled" to something meaningful.
3. Add the data points to the curve.

A curve can be removed by selecting the curve and then clicking on the `Remove` button. Models defined in this manner will be added to the `nonLinearCurves.strd` file found in the Strata installation folder.

Temporary Models

If you want to define a curve without adding it to the library of models, simply select `Custom` from the drop-down list. Changing to the `Custom` model does not clear the previous models data which allows for a model to be modified.

4.1.4 Recorded Motion Dialog

The `Recorded Motion Dialog` is used to load a recorded motion into Strata and appears when the `Add` button is clicked in the `Record Motion(s)` table. The dialog, shown in Figure 4.4 allows the user to load a variety of motions in most formats using the following steps:

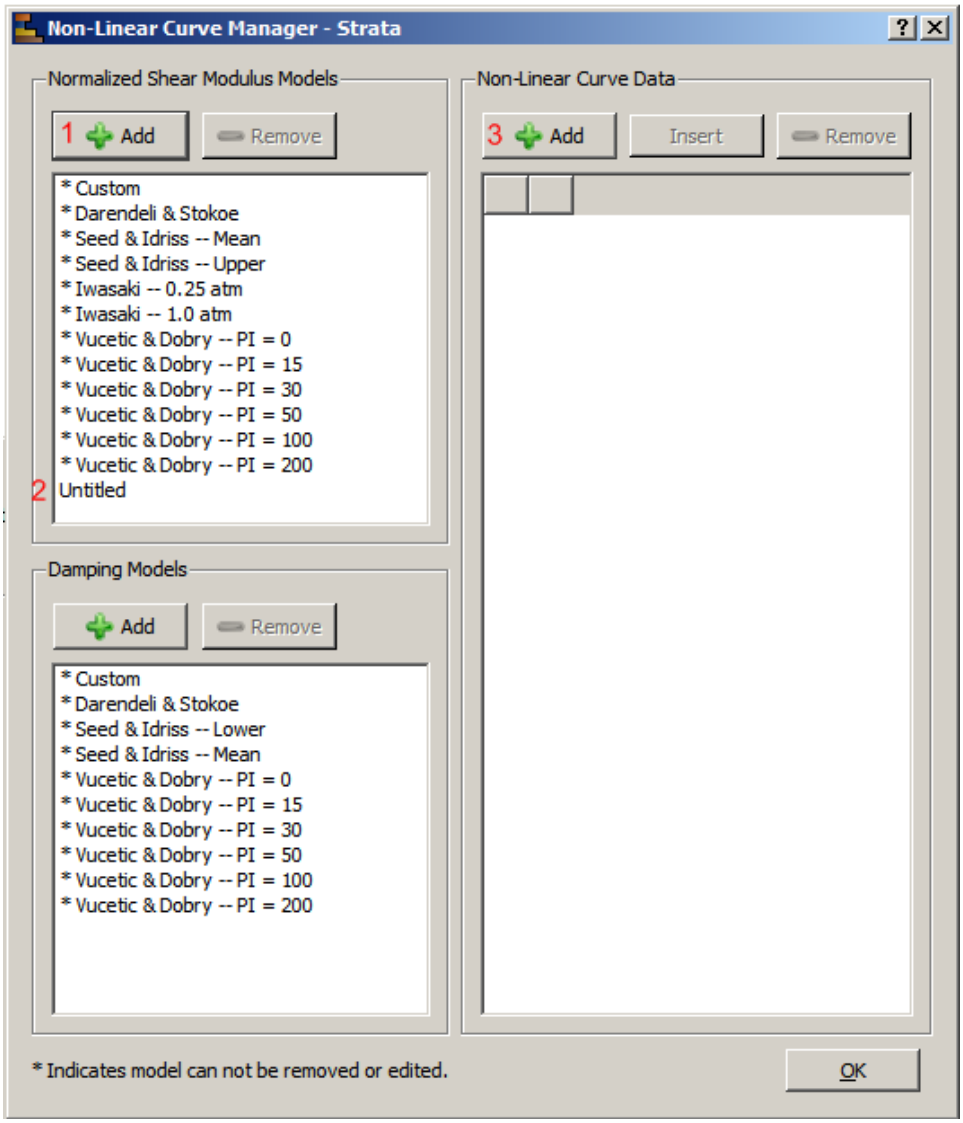

Figure 4.3: The nonlinear curve manager.

1. Click on the `File...` button and select the acceleration time series file. If the file is from the NGA database, then the remainder of the form will be automatically completed as shown in Figure 4.5. Regardless of the file type, the file is read and loaded into the preview area.

2. The remaining fields need to be filled to reflect the information in the file. Information is required for all fields except for the `Description` field. Fields can be completed by either typing values in, or selecting from the file preview and dragging the selected text into the field. The `Start line` and `Stop line` control which lines in the file contain the data. A zero value for the `Stop line` will result in the data being read until the end of the file. The file preview can be colored by clicking on the `Refresh` button. The colors have the following meanings:

   green text found prior to the acceleration-time series data (ignored).

   blue acceleration-time series data

   red text after the time series data (ignored).

   An example of the colored data is shown in Figure 4.5.

3. The scale factor can be selected at this time or after the motion has been loaded. *The scale factor should result in the motion being in units of gravity*. After the motion has been loaded, the scale factor can also be adjusted by setting the peak-ground acceleration.

4. After the form has been completed, the time-series can be viewed by clicking on the `Plot` button.

5. Click `OK` to finish loading the file.

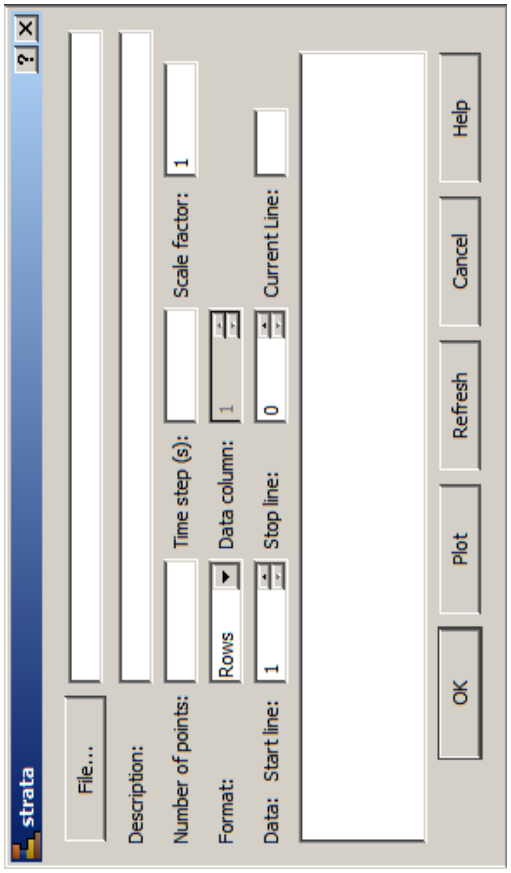

Figure 4.4: The initial view of the `Recorded Motion Dialog`.

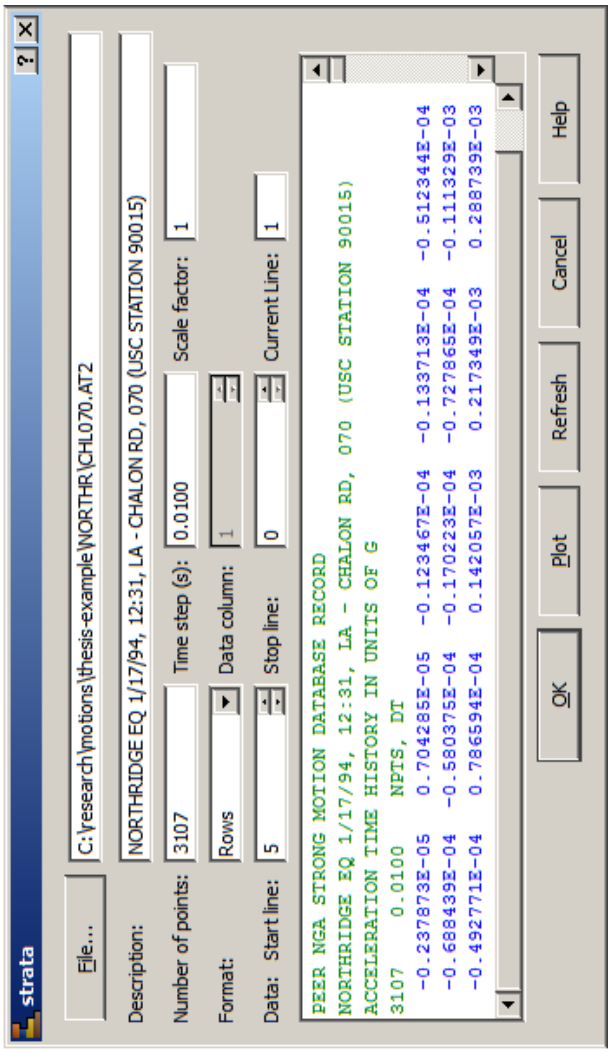

Figure 4.5: An example a completed `Recorded Motion Dialog`.

4.1.5 Output Widget

Once the site response calculation has been completed the view will change to the `Output Widget`. The `Output Widget` is also selected if a Strata output file is opened, or by selecting `Output View` from the `Window` menu.

Strata does not output any data files automatically. The data can also be exported by selecting `Export...` from the `File` menu. The exported data file is in a comma-separated values (CSV) format that can be easily opened with Excel or other spreadsheet program. All data (even disabled results) are included in the files.

Each result is characterized by a site realization and a motion. If the data is enabled, the check box with be checked, otherwise it is considered disabled. Results that are enabled will be included when the statistics are calculated. At the bottom of the table there are two buttons that allow all motions or sites related to the currently selected result to be enabled or disabled. In the example (Figure 4.6), both the site and motion are enabled. Whenever the status of a result is changed (e.g. from disabled to enabled) the `Recompute Statistics` button will become enabled allowing the user to update the median and standard deviation.

The `Output Widget` shown in Figure 4.6 is used to examine the results of a calculation. In the figure, the output is acceleration response spectrum computed at the surface for 20 motions and 20 different site profiles. A individual result can be selected by either clicking on the corresponding in the `Data Selection` table, or by clicking on the result in the plot. In both cases, the result is colored green if the result is enabled, or red if the result is disabled. After the status of a result has been changed, the `Recomputed Statistics` button will become enabled indicating that the median and standard deviation (shown on the plot in solid and dash blue lines, respectively) need to be updated.

The current plot can be printed by selecting `Print...` or `Print to PDF...` from the `File` menu. The current plot can also be copied by right clicking on the plot and selecting `Copy`.

4.2 Examples

The following examples give a basic introduction to using Strata to perform equivalent linear site response analysis. The examples files are found within the `examples` folder in the installation path. The examples can be opened by either double clicking on their file, or selecting them from the `Open...`

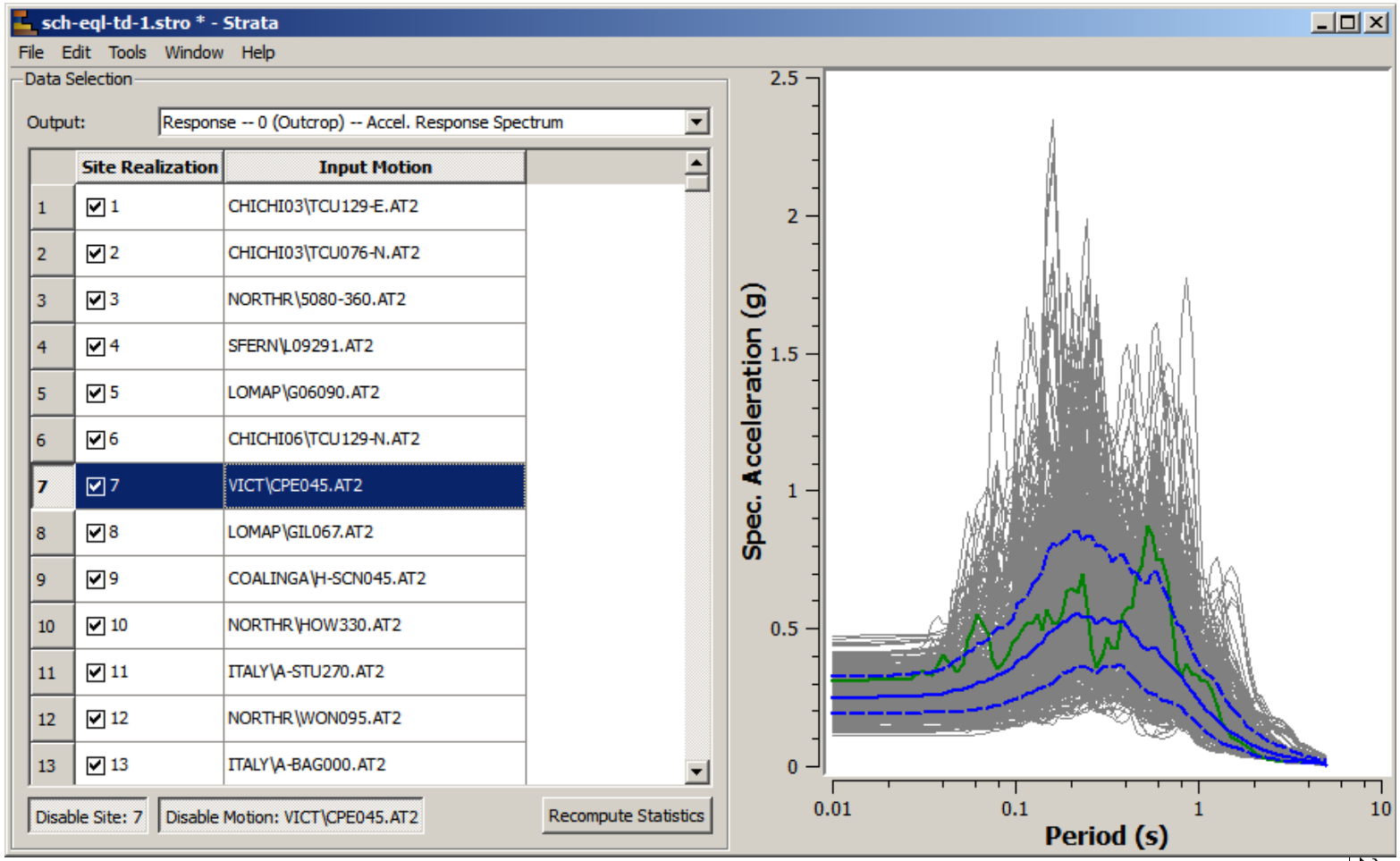

Figure 4.6: Using the Output view to examine the results of a calculation.

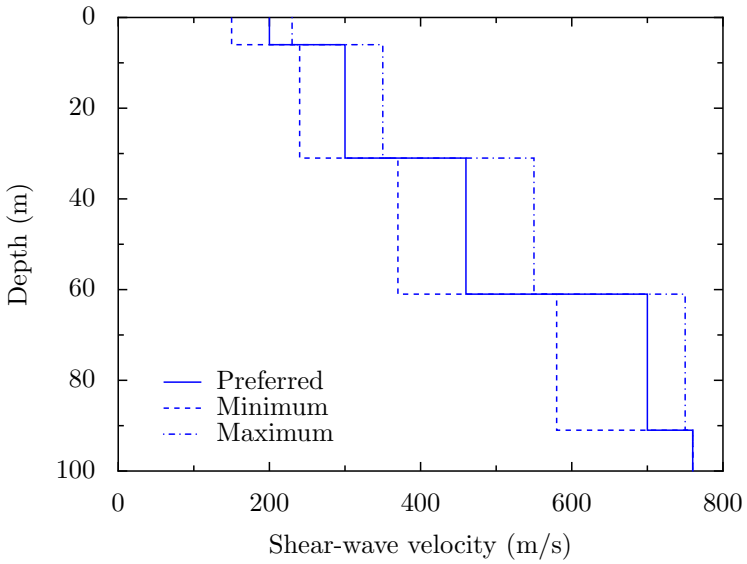

Figure 4.7: The shear-wave velocity profile of the Sylmar County Hospital Parking Lot site (Chang, 1996).

item from the `File` menu.

All examples use the deep alluvium Sylmar County Hospital Parking Lot (SCH) site located in Southern California for the site profile. The soil types and velocity layering of the site was proposed by Chang (1996). The soil properties are listed in Table 4.1 with a water table at a depth of 46 meters. The nonlinear properties for each of the layers were computed using the Darendeli (2001) empirical model with PI=0, OCR=1, and the confining pressures listed in Table 4.1. The corresponding velocity profile is shown in Figure 4.7. The time-averaged shear-wave velocity over the top 30 meters was computed as 273 m/s which classifies the site as a USGS site class C.

4.2.1 Example 1: Basic time domain

In the first example, the site response will be computed for the Sylmar County Hospital Parking Lot site using seven different recorded motions. This example can be opened from the `example-1-td.stri` file in the `examples` directory. Strata has the option of saving the time-series data within the project file which is useful when the project files is transferred to different

Depth Range (m)	**Soil Type**	$\mathbf{V_s}$ (m/s)	$\gamma_{\mathbf{tot}}$ (kN/m^3)	σ'_v (kPa)	σ'_m (atm)
0 to 6	Alluvium (Sand)	200 (150 to 230)	18	54	0.36
6 to 31	Alluvium (Sand)	300 (240 to 350)	18	222	2.2
31 to 61	Alluvium (Sand)	460 (370 to 550)	19	562	5.6
61 to 91	Alluvium and Older Alluvium (Sand)	700 (580 to 750)	22	776	7.7
91+	Bedrock	760	22		

Table 4.1: Soil profile at the Sylmar County Hospital Parking Lot site (Chang, 1996). The mean effective stress (σ'_m) is computed assuming a k_0 of 1/2 and a water table depth of 46 meters.

computers. For this example, the acceleration-times series are included in the project file. While the different tabs in the project can be accessed in any order, going from left-to-right is preferred as information in one tab may depend on tabs to the left of it.

Defining soil types

A soil type is defined by a name, unit weight, an initial damping, shear-modulus reduction model, damping model, and notes about the soil type. The name is only used to identify the soil type, and the notes are only present to type maintain sanity. For soil types that use the Darendeli (2001) model for either of nonlinear properties, addition properties required by the empirical model must be defined.

For the site profile presented in Table 4.1, four different soil types are required. Each soil type uses the Darendeli (2001) model for both the shear-modulus reduction and damping, but the mean effective stress in the model changes.

Defining soil profile

The soil profile combines the shear-wave velocity profile and soil types together. For each soil layer in the profile, requires that a thickness, soil type, and shear-wave velocity must be assigned. The soil types are selected from a list of soil types defined in the `Soil Types` tab.

Defining the acceleration-time series

The example provides seven acceleration-time series scaled to a target response spectrum and standard deviation. A motion is added by clicking on the `Add` button in the `Recorded Motion(s)` table. After clicking add a dialog will appear to assist in loading the file, information on this dialog is presented in Section 4.1.4. Once the motion has been loaded, only the scale factors can be changed by either specifying a peak-ground acceleration or a scale factor. If the `Save motion data with the input file` check box is checked, then the Strata input file will contain all of the information regarding the time series. This increases the size of the input file, but allows for a single file to contain all required input.

Defining the output

There are generally four different types of output that can be computed by Strata:

Response location output involves the response at a given location (e.g. acceleration response spectrum or a time series).

Ratio output involves the ratio of a response at two different location at a given location (e.g. transfer function or spectral ratio).

Profile variation of a property with depth (e.g. maximum shear-strain). The profiles are computed at particular depths because the layering of the model may change as a result of variation.

Non-linear curves the nonlinear curves.

Note: Only the information requested is stored.

Computing

After the project is fully defined, switch the `Compute` tab and click on the `Compute` button. Information regarding the calculation will be displayed in the window and once the calculation is complete the view will switch to the output widget. For more information on using the output widget see Section 4.1.5. The input widget can be selected by selected `Input View` from the `Window` menu, or by pressing `F2`.

4.2.2 Example 2: RVT and Site Variation

In the second example, the site response for the SCH site using random vibration theory and variation of the shear-wave velocity profile. This example can be opened from the `example-2-rvt.stri` file in the `examples` directory. The site profile is exactly the same as was used in the previous example. There are only two changes that will be discussed: the change from time domain to random vibration theory, and how to enable site variation. Both of these settings are enabled in the `General Settings` tab. Figure 4.8 shows the proper settings for enabling RVT and shear-wave velocity variation.

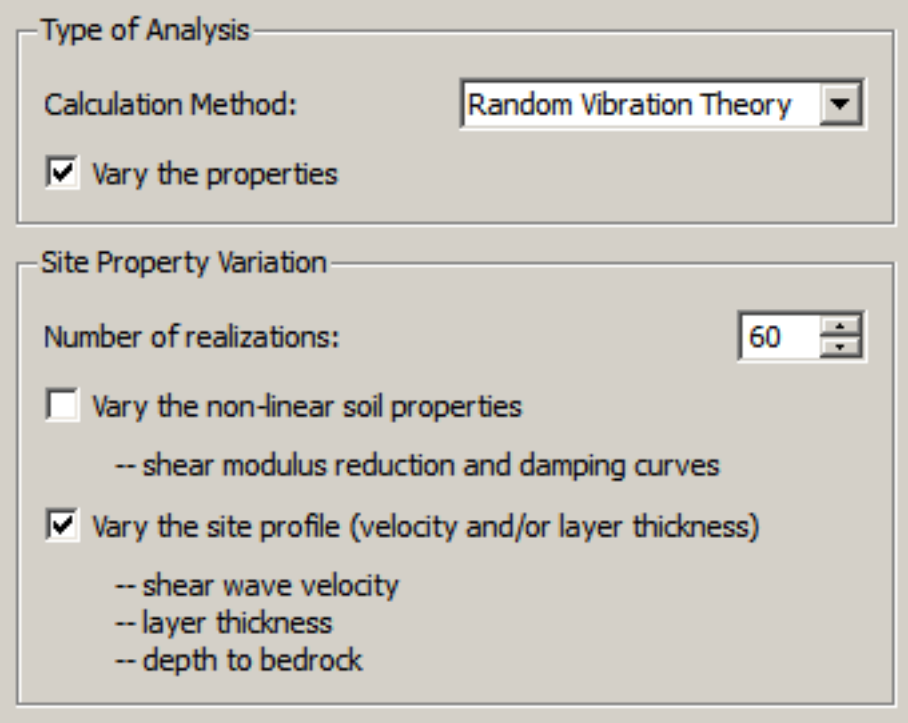

Figure 4.8: Settings to enable RVT site response and variation of the shear-wave velocity.

Varying the shear-wave velocity

The parameters that control the shear-wave velocity variation are found on the `Soil Profile` tab. By enabling variation of the site profile a number of new columns will appear in the velocity layers table, as well as a new group box containing a number of properties to vary. In this example, only the shear-wave velocity will be varied using the `USGS C` parameters for both the standard deviation and correlation models.

Defining an input acceleration response spectrum

Random vibration theory allows for the input motion to be defined using either a Fourier amplitude spectrum (FAS) or an acceleration response spectrum. In this example, a response spectrum was computed using Abrahamson and Silva (1997) empirical model for a magnitude 7.0 earthquake

generated by a strike-slip fault with a distance of 20 km. The duration of the event was computed uses the Abrahamson and Silva (1996) empirical relationship for the duration using an normalized Arias intensity of 0.75. Whenever a response spectrum is used for input it is important to check that the resulting FAS looks appropriate. Strata allows the user to see both the data and the plots of the data prior to the calculation.

Bibliography

N. A. Abrahamson and W. J. Silva. Empirical ground motion models. Technical report, Brookhaven National Laboratory, Upton, New York, 1996.

N. A. Abrahamson and W. J. Silva. Empirical response spectral attenuation relations for shallow crustal earthquakes. *Seismological Research Letters*, 68(1):94–127, January-Feburary 1997.

A. H.-S. Ang and W. H. Tang. *Probability Concepts in Engineering Planning and Design: Volume I–Basic Principles*. John Wiley and Sons, New York, 1975.

A. H.-S. Ang and W. H. Tang. *Probability Concepts in Engineering Planning and Design: Volume II–Descision, Risk, and Reliability*. Ang and Tang, 1990.

D. Boore. Simulation of ground motion using the stochastic method. *Pure and Applied Geophysics*, 160(3-4):635–676, March 2003.

D. M. Boore and W. B. Joyner. A note on the use of random vibration theory to predict peak amplitudes of transient signals. *BSSA*, 74(5):2035–2039, October 1984.

J. N. Brune. Tectonic stress and the spectra of seismic shear waves from earthquake. *Journal of Geophysics Research*, 75(26):4997–5009, 1970.

J. N. Brune. Correction. *Journal of Geophysics Research*, 76:5002, 1971.

K. W. Campbell. Prediction of strong ground motion using the hybrid empirical method and its use in the development of ground-motion (attenuation) relations in the Eastern North America. *BSSA*, 93(3):1012–1033, June 2003.

D. Cartwright and M. S. Longuet-Higgins. The statistical distribution of the maxima of a random function. *Proceedings of the Royal Soceity of London, Series A, Mathematical and Physical Sciences*, 237(1209):212–232, 1956.

S. W.-Y. Chang. *Seismic response of deep stiff soil deposits*. PhD thesis, University of California, Berkeley, December 1996.

C. Costantino, E. Heymsfield, and Y. Gu. Site specific estimates of surface ground motions for the K-reactor site, Savannah River plant. Report CEERC-91-003, Structural Analysis Division, Nuclear Energy Department, Brookhaven National Laboratory, Upton, NY, 1991.

M. B. Darendeli. *Development of a new family of normalized modulus reduction and material damping curves*. PhD thesis, The University of Texas, Austin, 2001.

D. A. Gasparini and E. H. Vanmarcke. Simulated earthquake motions compatible with prescribed response spectra. Technical Report R76-4, Massachusetts Institute of Technology, Cambridge, MA, 1976.

B. O. Hardin and V. P. Drnevich. Shear modulus and damping in soils: design equations and curves. *Journal of soil mechanics and foundation engineering division, ASCE*, 98(SM7):667–692, June 1972.

I. M. Idriss and J. I. Sun. *SHAKE91: a computer program for conducting equivalent linear seismic response analyses of horizontally layered soil deposits*. Center for Geotechnical Modelling, Department of Civil and Environmentall Engineering, University of California, Davis, 1992.

T. Iwasaki, F. Tatsuoka, and Y. Takagi. Dynamic shear deformation properties of sand for wide strain range. Technical Report 1085, Civil Engineering Institue, Ministry of Construction, Tokyo, Japan, 1976.

S. L. Kramer. *Geotechnical Earthquake Engineering*. Prentice Hall, Upper Saddle River, NJ, 1996.

R. McGuire, G. Toro, T. O'Hara, J. Jacobson, and W. Silva. Probablistic seismic hazard evaluations at nuclear plant sites in the Central and Eastern United States: Resolution of the Charleston Earthquake issue. Technical Report NP-6395-D, Electric Power Research Institute, Palo Alto, CA, April 1989.

E. M. Rathje, A. R. Kottke, and C. M. Ozbey. Using inverse random vibration theory to develop input Fourier amplitude spectra for use in site response. In *16th International Conference on Soil Mechanics and Geotechnical Eningeering: TC4 Earthquake Geotechnical Engineering Satellite Conference*, pages 160–166, Osaka, Japan, September 2005.

P. B. Schnabel, J. Lysmer, and H. B. Seed. Shake: A computer program for earthquake response analysis of horizontally-layered sites. Technical Report EERC-72/12, Earthquake Engineering Research Center, University of California, Berkeley, CA, 1972.

J. F. Schneider, W. J. Silva, S. J. Chiou, and J. C. Stepp. Estimation of ground motion at close distances using the band-limited-white-noise model. In *Fourth Interntional Conference on Seismic Zonation*, volume 4, pages 187–194, Stanford, CA, 1991. EERI.

H. B. Seed and I. M. Idriss. Soil moduli and damping factors for dynamic response analyses. Technical Report EERC 70-10, Earthquake Engineering Research Center, University of California, Berkeley, CA, 1970.

W. J. Silva, N. Abrahamson, G. Toro, and C. Costantino. Description and validation of the stochastic ground motion model. Final Report Contract No. 770573, Brookhaven National Laboratory, Upton, N.Y., 1997.

G. Toro, W. Silva, R. McGuire, and R. Hermann. Probabilistic seismic hazard mapping of the Mississippi Embayment. *Seismological Research Letters*, 63 (3):449–475, July-September 1992.

G. R. Toro. Probablistic models of site velocity profiles for generic and site-specific ground-motion amplification studies. Technical Report 779574, Brookhaven National Laboratory, Upton, New York, 1995.

E. Vanmarcke. *Random fields, analysis and synthesis*. The MIT Press, Cambridge, Massachusetts, 1983.

M. Vucetic and R. Dobry. Effect of soil plasticity on cyclic response. *Journal of the Geoechnical Engineering Division, ASCE*, 117(1):89–107, 1991.

Index

fast Fourier transform, 15

motion type
    outcrop, 5
    within, 6

Nyquist frequency, 15

random vibration theory
    Parseval's theorem, 18
    peak factor, 18
    response spectrum inversion, 20

shear modulus
    complex, 3
    maximum (small strain), 8

transfer function
    acceleration, 5
    strain, 8

wave equation, 2